

1 Inside Dynamics for Stage-Structured Integrodifference Equations

2 Nathan G. Marculis · Jimmy Garnier · Roger Lui ·
3 Mark A. Lewis

4
5 Received: date / Accepted: date

6 **Abstract** A stage-structured model of integrodifference equations is used to study the asymptotic neutral
7 genetic structure of populations undergoing range expansion. That is, we study the inside dynamics of
8 solutions to stage-structured integrodifference equations. To analyze the genetic consequences for long term
9 population spread, we decompose the solution into neutral genetic components called neutral fractions.
10 The inside dynamics are then given by the spatiotemporal evolution of these neutral fractions. We show
11 that, under some mild assumptions on the dispersal kernels and population projection matrix, the spread
12 is dominated by individuals at the leading edge of the expansion. This result is consistent with the founder
13 effect. In the case where there are multiple neutral fractions at the leading edge we are able to explicitly cal-
14 culate the asymptotic proportion of these fractions found in the long-term population spread. This formula
15 is simple and depends only on the right and left eigenvectors of the population projection matrix evaluated
16 at zero and the initial proportion of each neutral fraction at the leading edge of the range expansion. In
17 the absence of a strong Allee effect, multiple neutral fractions can drive the long-term population spread,
18 a situation not possible with the scalar model.

19 **Keywords** integrodifference equations · stage-structure · inside dynamics · neutral genetic structure ·
20 founder effect

21 **Mathematics Subject Classification (2000)** 39A10 · 45G10 · 92D25 · 92D40

22 1 Introduction

23 There are a wide array of observational (Cullingham et al. 2011), empirical (Liebhold et al. 1992; Lubina
24 and Levin 1988), and theoretical studies (Li et al. 2009; Lui 1989a; Weinberger 1982) for the spatial spread
25 of populations by range expansion. Over the last decades, theoretical studies about range expansion mainly

This research was supported by a grant to MAL from the Natural Science and Engineering Research Council of Canada (Grant No. NET GP 434810-12) to the TRIA Network, with contributions from Alberta Agriculture and Forestry, Foothills Research Institute, Manitoba Conservation and Water Stewardship, Natural Resources Canada-Canadian Forest Service, Northwest Territories Environment and Natural Resources, Ontario Ministry of Natural Resources and Forestry, Saskatchewan Ministry of Environment, West Fraser and Weyerhaeuser. MAL is also grateful for support through NSERC and the Canada Research Chair Program. NGM acknowledges support from NSERC TRIA-Net Collaborative Research Grant. JG acknowledges NONLOCAL project (ANR-14-CE25-0013) and the European Research Council (ERC) under the European Unions Horizon 2020 research and innovation programme (grant agreement No 639638, MesoProbio). The authors also gratefully acknowledge the helpful suggestions from the anonymous reviewers.

Nathan G. Marculis
Department of Mathematical and Statistical Sciences, University of Alberta, Edmonton, AB T6G 2G1, Canada
E-mail: marculis@ualberta.ca

Jimmy Garnier
Université Savoie MontBlanc, CNRS, LAMA, F-73000 Chambéry, France

Roger Lui
Department of Mathematical Sciences, Worcester Polytechnic Institute, Worcester, MA 01609, USA

Mark A. Lewis
Department of Mathematical and Statistical Sciences, University of Alberta, Edmonton, AB T6G 2G1, Canada
Department of Biological Sciences, University of Alberta, Edmonton, AB T6G 2G1, Canada

26 focused on the asymptotic speed of propagation of the expanding population or the profile of invasion
 27 (Hastings et al. 2005). Spatial models in population genetics have also been developed for studying the
 28 spread of an advantageous gene in a population (Lui 1982a,b, 1983; Weinberger 1978, 1982). Recently,
 29 much effort have been invested to understand the genetic consequences of range expansion (Hallatschek
 30 and Nelson 2008; Roques et al. 2012). Indeed, range expansions are known to have significant effects on
 31 genetic diversity (Davis and Shaw 2001; Hewitt 2000). For instance, if range expansion occurs through
 32 successive founder effects, genetic diversity is likely to decrease. However, empirical and theoretical studies
 33 have shown that many mechanisms may reduce or reverse the loss of diversity in an expanding population
 34 (Pluess 2011). In particular, the presence of an Allee effect (Roques et al. 2012) which reduces the per-capita
 35 growth rate at low density, the occurrence of long distance dispersal events (Bonnefon et al. 2014; Ibrahim
 36 et al. 1996), or the existence of a juvenile stage (Austerlitz and Garnier-Géré 2003) may promote neutral
 37 genetic diversity in traveling waves of colonization. In this work, we are interested in the neutral genetic
 38 dynamics of a stage-structured population undergoing range expansion.

39 It is well known that the structure of the population is important for understanding the asymptotic
 40 dynamics. For example, individuals often must undergo a maturation period before they can produce off-
 41 spring. For discrete population models, the dynamics of the life history traits have typically been structured
 42 according to age, Leslie matrix (Leslie 1945), or developmental stage, Lefkovich matrix (Lefkovich 1965),
 43 but matrix models can be easily generalized to include other physiological characteristics. It is also com-
 44 mon for sessile species to typically have a motile stage in their development, such as seed dispersal in plant
 45 populations (Howe and Smallwood 1982) and larval dispersal in marine environments (Levin 2006).

46 Our study considers a stage-structured integrodifference equation describing range expansion for a
 47 population of the form:

$$\mathbf{u}_{t+1}(x) = \int_{-\infty}^{\infty} [\mathbf{K}(x-y) \circ \mathbf{B}(\mathbf{u}_t(y))] \mathbf{u}_t(y) dy, \quad (1)$$

48 where $\mathbf{u}_t(x)$ corresponds to the population density at time t and location x . The population is structured
 49 into m stages, whose densities are given by $\mathbf{u}_t(x) = [u_{1,t}(x), \dots, u_{m,t}(x)]$. Each stage distribution changes
 50 in time and space through the successive effects of dispersal, described by the dispersal matrix $\mathbf{K} = [k_{jl}]$,
 51 and the demography, embodied in the population projection matrix $\mathbf{B}(\mathbf{u}) = [b_{jl}(\mathbf{u})]$ which takes into
 52 account density-dependence. The succession of the reproduction stage and dispersal stage is described by
 53 the Hadamard product \circ (element-wise multiplication of matrix). This model allows the different stages to
 54 spread, reproduce, and interact in a variety of ways that cannot be captured by scalar models (Neubert and
 55 Caswell 2000). More precisely, if we consider stage j , where $j = 1, \dots, m$, then its density, $u_{j,t}(x)$, satisfies
 56 the following equation

$$u_{j,t+1} = \int_{-\infty}^{\infty} \sum_{l=1}^m k_{jl}(x-y) b_{jl}(u_{1,t}(y), \dots, u_{m,t}(y)) u_{l,t}(y) dy \quad (2)$$

57 where $k_{jl}(x-y) dy$ is the probability that an individual transitioning from stage l to stage j disperses from
 58 the interval $(y, y+dy]$ to location x , and the function b_{jl} is the per-capita production of stage j individuals
 59 from stage l individuals. Such a model has been used to describe epidemic spread (Lui 1989b), biological
 60 invasions (Bateman et al. 2017; Veit and Lewis 1996), and critical domain size (Lutscher and Lewis 2004).

61 The model (1) is biologically valid if the stages are chosen in a way such that the life history and
 62 dispersal parameters vary within stages as little as possible. In some cases this is easy; for example, a
 63 division between juvenile and adult individuals is normally determined by the ability to reproduce. In other
 64 cases, the division may not be so clear, and partitions may be difficult to decide. Fortunately, there are
 65 algorithms that can be used to minimize errors associated with partitioning a population into distinct stages
 66 (Moloney 1986; Vandermeer 1978). If the division of population structure is modeled using a continuous
 67 variable such as size or mass, and there is no natural break point to structure the population into distinct
 68 stages then an integral projection model may be more appropriate (Easterling et al. 2000).

69 The goal of this work is to understand the neutral genetic patterns of structured populations. Neutral
 70 genetic markers are genes that have no direct effect on individual fitness. Even though this type of gene
 71 tells us nothing about the adaptive or evolutionary potential of a population, neutral genetic markers can
 72 be used to understand processes such as gene flow, genetic drift, migration, or dispersal (Holderegger et al.
 73 2006). It has also been shown by simulations that high levels of neutral genetic diversity can be correlated
 74 with increased allelic richness at loci under selection (Bataillon et al. 1996). Our analysis will be focused
 75 on the inside dynamics of stage-structured integrodifference equations.

76 This paper is organized as follows. Section 2 is dedicated to providing necessary background material
 77 for understanding the main results. Within this section, we break it into two subsections: Section 2.1

78 provides background to the analysis of inside dynamics and the stage-structured integrodifference equation
79 used in our analysis and Section 2.2 lays out four of the major assumptions made about the demographic
80 and dispersal processes. In Section 3, we provide asymptotic results regarding population structure. This
81 section is broken into three parts. Section 3.1 covers the inside dynamics of neutral fractions not present
82 at the leading edge, Section 3.2 discusses the inside dynamics of neutral fractions that are located at the
83 leading edge, and Section 3.3 contains proofs for our main theorems. To complement the analytical results,
84 numerical simulations are given in Section 4. Finally, in Section 5, we discuss the modeling technique,
85 results, numerical simulations, and implications of our work.

86 2 Materials and methods

87 2.1 Inside dynamics

88 To study the neutral genetic distribution of a population, we consider the inside dynamics of the population.
89 The term inside dynamics refers to the inside structure of the population rather than the total density.
90 The key assumption in the analysis of inside dynamics is that all individuals grow and disperse in the
91 same manner, differing only with respect to neutral genetic markers. In other words, all individuals in the
92 population have the same fitness. This allows us to split up the population into distinct subgroups called
93 neutral fractions with which we track the spatiotemporal evolution of these subgroups.

94 Inside dynamics have been studied for reaction-diffusion equations (Garnier and Lewis 2016; Garnier
95 et al. 2012; Roques et al. 2012), delay reaction-diffusion equations (Bonnefon et al. 2013), integro-differential
96 equations (Bonnefon et al. 2014), and integrodifference equations (Lewis et al. 2018; Marculis et al. 2017).
97 In these works, the subject for analysis was a scalar population model. Indeed, to date, there is only one
98 study of the inside dynamics of systems of equations. This study concentrated on the analysis on a diffusive
99 Lotka-Volterra competition system (Roques et al. 2015). Our mathematical contribution to this area of
100 research is to extend the analysis of inside dynamics to stage-structured integrodifference equations.

101 Recall the stage-structured population model in (1). Separating the initial population up into distinct
102 neutral fractions, we obtain the initial condition

$$\mathbf{u}_0(x) = \sum_{i=1}^n \mathbf{v}_0^i(x), \quad (3)$$

103 where $\mathbf{v}_0^i(x) \geq 0$ is the initial population density for neutral fraction i and n is the finite number of neutral
104 fractions. An illustration of this decomposition can be seen in Figures 1(a) and 2(a). By assuming that
105 individuals in each neutral fraction grow and disperse similarly, we obtain the following system of equations:

$$\mathbf{v}_{t+1}^i(x) = \int_{-\infty}^{\infty} [\mathbf{K}(x-y) \circ \mathbf{B}(\mathbf{u}_t(y))] \mathbf{v}_t^i(y) dy, \quad i = 1, \dots, n, \quad (4)$$

106 where $\mathbf{u}_t(y) = \sum_{i=1}^n \mathbf{v}_t^i(y)$. Throughout the remaining sections, we use the superscript i to denote the
107 neutral fraction and, when not written in vector form, subscript j to denotes the stage. Note that the
108 number of neutral fractions, n , and the number of stages in the population, m , need not be the same
109 ($n \neq m$). Also, observe the model given in Equation (4) is natural extension of the scalar model to a system
110 of recursions (Marculis et al. 2017). Thus, it can be expected that many of the results proven for the scalar
111 equation can be extended to systems of cooperative equations. This is the approach we take in what follows.

112 2.2 Demographic and dispersal assumptions

113 For each of our main theorems, we make five assumptions regarding Equations (3)-(4). The first three as-
114 sumptions are related to the population projection matrix, the fourth assumption is related to the dispersal
115 kernel, and the fifth and final assumption is related to the decay of the initial conditions. In this section,
116 we outline the first four assumptions related to the demography and dispersal of the population.

117 *Population projection matrix*

118 We begin with looking at the population projection matrix $\mathbf{B}(\mathbf{u})$. Here, we outline three assumptions about
 119 the population projection matrix. The population projection matrix describes reproduction, survival, and
 120 interactions between stages. As a projection matrix, its entries should be nonnegative:

121 *A1 : The matrix $\mathbf{B}(\mathbf{u})$ is nonnegative for any $\mathbf{u} \in (0, \infty)^m$.*

122 Moreover, we can see from (1) that $\mathbf{0}$ is a steady state of the problem. Define

$$\mathbf{B}_0 := \mathbf{B}(\mathbf{u})|_{\mathbf{u}=\mathbf{0}}. \quad (5)$$

123 Notice that \mathbf{B}_0 is the population projection matrix evaluated at $\mathbf{u} = \mathbf{0}$. We will assume that this steady
 124 state is unstable. More precisely, we assume:

125 *A2 : \mathbf{B}_0 is a primitive matrix, that is there exists $k > 0$ such that \mathbf{B}_0^k is positive, and its dominant
 126 eigenvalue, λ_1 , is greater than 1, $\lambda_1 > 1$.*

127 Finally, we assume that there are no Allee effects. That is:

128 *A3 : $\mathbf{B}(\mathbf{u})$ is bounded by its linearization at the steady state $\mathbf{0}$, $\mathbf{B}(\mathbf{u})\mathbf{v} \leq \mathbf{B}_0\mathbf{v}$ for all $\mathbf{v} \in (0, \infty)^m$.*

129 *Dispersal kernel*

130 In our model, we assume that individuals in the population may disperse at long distance but those events
 131 are rare in the following sense:

132 **Definition 1** *A dispersal kernel, $k(x)$, is called thin-tailed if there exists a $\xi > 0$, such that*

$$\int_{-\infty}^{\infty} k(x)e^{\xi|x|} dx < \infty. \quad (6)$$

133 A dispersal kernel that is not thin-tailed is called a fat-tailed dispersal kernel, and in this case, the long
 134 distance dispersal events become frequent, which leads to different behaviors for some solutions, such as
 135 accelerating waves. Many of the classical mathematical results for (1), such as traveling wave solutions
 136 and the asymptotic speed of propagation, rely on the assumption that the dispersal kernel is thin-tailed. A
 137 common dispersal kernel that we consider throughout our work is the Gaussian probability density function:

$$k(x; \mu, \sigma) = \frac{1}{\sqrt{2\pi\sigma^2}} e^{-\frac{(x-\mu)^2}{2\sigma^2}}, \quad (7)$$

138 where μ is the mean shift in location and σ^2 is the variance in dispersal distance. In the following sections,
 139 we use the following shorthand notation to denote that the dispersal kernel is Gaussian by k is $N(\mu, \sigma^2)$.
 140 In what follows, we will make one of two assumptions about the dispersal kernels.

141 *A4 : Each kernel, $k_{ji}(x - y)$, is thin-tailed.*

142 *A4' : Each kernel, $k_{ji}(x - y)$, is $N(\mu, \sigma^2)$.*

143 From above, we see that our fourth assumption provides a condition on the dispersal kernels. In both cases,
 144 we assume, at a minimum, that every dispersal kernel is thin-tailed in order to calculate the asymptotic speed
 145 of propagation. The above assumption implies that we are not considering a population with accelerating
 146 waves (Kot et al. 1996).

147 *Asymptotic speed of propagation*

148 Under the previous assumptions A1-A4 we can deduce from the work of Lui (1989a) that solutions of (1)
 149 will spread to the right with an asymptotic spreading speed c greater than or equal to a critical spreading
 150 speed $c^* > 0$ for appropriately chosen initial conditions. Moreover, the critical spreading speed c^* can be
 151 computed explicitly by the following formula

$$c^* := \min_{0 < s < s^+} \frac{1}{s} \ln \rho(s), \quad (8)$$

152 where $\rho(s) := \rho(\mathbf{H}(s)) > 1$ is the dominant eigenvalue of $\mathbf{H}(s)$ defined by

$$\mathbf{H}(s) := \mathbf{M}(s) \circ \mathbf{B}_0. \quad (9)$$

153 The moment generating function matrix $\mathbf{M}(s)$ is calculated by applying the reflected bilateral Laplace
 154 transform to the dispersal kernel matrix \mathbf{K} and is defined by

$$\mathbf{M}(s) := \int_{-\infty}^{\infty} \mathbf{K}(x)e^{sx} dx. \quad (10)$$

155 Since the entries of the dispersal kernel matrix, k_{jl} , are thin-tailed by Assumption A5, this matrix is well
 156 defined over $(0, s^+)$ where $s^+ \in (0, \infty]$. Throughout our analysis, we let $s_0(c)$ be the smallest positive root
 157 of the equation

$$cs = \ln(\rho(s)) \text{ for } c \geq c^*. \quad (11)$$

158 We know that $s_0(c)$ exists because $\rho(s)$ is log convex; see Lemma 6.4 by Lui (1989a). In particular, when
 159 each kernel is Gaussian, k_{jl} is $N(\mu, \sigma^2)$, then we have an explicit formula for the asymptotic speed of
 160 propagation given by

$$c^* = \sqrt{2\sigma^2 \ln(\lambda_1)} + \mu, \quad (12)$$

161 where λ_1 is the dominant eigenvalue of \mathbf{B}_0 and we can explicitly compute $s_0(c)$ to be

$$s_0(c) = \frac{c - \mu + \sqrt{(c - \mu)^2 - 2\sigma^2 \ln(\lambda_1)}}{\sigma^2}. \quad (13)$$

162 The technical details for the asymptotic speed of propagation are provided in Appendix A.

163 3 Main results

164 Henceforth, we assume that the structured population, $\mathbf{u}_t(x)$, satisfies (1) with an initial condition $\mathbf{u}_0(x)$.
 165 With such initial condition, the population is spreading to the right with an asymptotic speed of propaga-
 166 tion, c , greater than or equal to c^* , given by formula (8). We first consider neutral fractions that are not
 167 present at the leading edge of the solution and then afterwards consider neutral fractions that are at the
 168 leading edge of the expanding population.

169 Our fifth and final assumption places a requirement on the initial conditions for the neutral fractions.
 170 This requirement is closely connected to the decay rate of the solution for the population and determines
 171 whether or not an individual is at the leading edge of the population spread. In particular, we know that
 172 the traveling wave solution for the linearized equation is given by an exponential function and the decay
 173 rate defines the leading edge of the population. The technical details of whether or not a neutral fraction
 174 is located at the leading edge is defined in the statement of our main theorems. We do not explicitly
 175 write these out here, but rather save them for the statement of our theorems because this assumption takes
 176 different forms based on our assumptions. We are now ready to present our first two theorems, that provides
 177 sufficient conditions for when the density of neutral fractions converges to zero in the moving half-frame.

178 3.1 Inside dynamics not at the leading edge

179 **Theorem 3.1** *Let us assume that A1-A4 hold true. Let $\mathbf{v}_t^i(x)$ be a neutral fraction satisfying (4) with*
 180 *initial condition $\mathbf{v}_0^i(x)$ satisfying (3) that is not present at the leading edge of the expanding population, in*
 181 *the sense that*

$$182 \quad A5 : x^2 \mathbf{v}_0^i(x) e^{s_0(c)x} \in L^1(\mathbb{R}) \cap L^\infty(\mathbb{R}) \text{ for a given } c \geq c^*.$$

183 *Then, for any $A \in \mathbb{R}$, the density of neutral fraction i , $\mathbf{v}_t^i(x)$, converges to $\mathbf{0}$ uniformly as $t \rightarrow \infty$ in the*
 184 *moving half-frame $[A + ct, \infty)$.*

185 In summary, Theorem 3.1 provides sufficient conditions for neutral fractions in the population to ap-
 186 proach zero asymptotically. This result implies that the only neutral fractions that will contribute to the
 187 spread of the population are those that are initially at the leading edge. In this scenario, we observe an
 188 extreme founder effect for the population spread. For this proof, see Section 3.3.

189 By making a stronger assumption on the dispersal kernels, we are able to relax Assumption A5 on the
 190 initial conditions in Theorem 3.1. In particular, for the next theorem we assume that all dispersal kernels
 191 are Gaussian with the same mean and variance as given by Assumption A4' and the assumption on the
 192 initial condition becomes a simple integrability condition.

193 **Theorem 3.2** *Let us assume that A1-A3 and A4' hold true. Let $\mathbf{v}_t^i(x)$ be a neutral fraction satisfying (4)*
 194 *with initial condition $\mathbf{v}_0^i(x)$ satisfying (3) that is not present at the leading edge of the expanding population,*
 195 *in the sense that*

$$196 \quad A5' : \int_{-\infty}^{\infty} e^{\frac{c-\mu}{\sigma^2}y} \mathbf{v}_0^i(y) dy < \infty \text{ for a given } c \geq c^*.$$

197 *Then, for any $A \in \mathbb{R}$, the density of neutral fraction i , $\mathbf{v}_t^i(x)$, converges to $\mathbf{0}$ uniformly as $t \rightarrow \infty$ in the*
 198 *moving half-frame $[A + ct, \infty)$.*

199 In summary, Theorem 3.2 provides the same result as Theorem 3.1 but with different assumptions on
 200 the dispersal kernels and initial conditions. That is, Theorem 3.2 provides sufficient conditions for when
 201 the neutral fractions do not contribute to the population spread. Under Assumption A5', we see that the
 202 leading edge is determined by the decaying exponential $e^{-\frac{c-\mu}{\sigma^2}x}$. This condition is much different than those
 203 given by Assumption A5 in Theorem 3.1. As in the previous theorem, we also observe here that the only
 204 neutral fractions that will contribute to the spread of the population are those that are initially at the
 205 leading edge. For this proof, see Section 3.3.

206 The proof of Theorem 3.1 is more complicated than that of Theorem 3.2, even though the method of
 207 proof and conclusions are the same. The difference is due to the assumptions made about the dispersal
 208 kernels. In Theorem 3.1 we assume the dispersal kernels are thin-tailed and must use the definition of the
 209 inverse reflected bilateral Laplace transform. In Theorem 3.2 we assume all dispersal kernels are Gaus-
 210 sian with the same mean and variance. This assumption simplifies the proof because convolving Gaussian
 211 distributions results in another Gaussian.

212 If the initial conditions are all compactly supported, then all neutral fractions will satisfy Assumption
 213 A5 and A5' respectively in Theorems 3.1 and 3.2. If the initial conditions decay according to the traveling
 214 wave solution, then all neutral fractions except those at the leading edge will satisfy Assumption A5 and
 215 A5' in Theorems 3.1 and 3.2 respectively. This means that the only neutral fractions that we will see in
 216 the moving half-frame are those that were initially at the leading edge. However, Theorems 3.1 and 3.2 do
 217 not tell us anything about these neutral fractions.

218 3.2 Inside dynamics at the leading edge

219 In the next theorem, we look at initial data that decay slower than Assumption A5' in Theorem 3.2. Here
 220 we are able to calculate the asymptotic proportion of each neutral fraction provided we move at the slowest
 221 speed c^* .

222 **Theorem 3.3** *Let us assume that A1-A3 and A4' hold true. Let $\mathbf{v}_t^i(x)$ be a neutral fraction satisfying (4)*
 223 *with initial condition $\mathbf{v}_0^i(x)$ satisfying (3) that is present at the leading edge of the expanding population,*
 224 *in the sense that for $c = c^*$*

$$225 \quad A5'' : \mathbf{v}_0^i(x) = (\mathbf{p}_0^i \circ \mathbf{r}) e^{-\frac{c-\mu}{\sigma^2}x}, \text{ where } \mathbf{p}_0^i \text{ is the initial proportion for neutral fraction } i \text{ in each stage, } \mathbf{r} \text{ is}$$

$$226 \quad \text{the right eigenvector of } \mathbf{B}_0 \text{ corresponding to } \lambda_1.$$

227 *Then, for any $A \in \mathbb{R}$, the density of neutral fraction i , $\mathbf{v}_t^i(x)$, asymptotically approaches a proportion, p^i ,*
 228 *of the traveling wave for the linear equation as $t \rightarrow \infty$ in the moving half-frame $[A + ct, \infty)$. That is,*

$$\lim_{t \rightarrow \infty} \mathbf{v}_t^i(x_0 + ct) = e^{-\frac{c-\mu}{\sigma^2}x_0} \mathbf{r} \mathbf{p}^i \quad (14)$$

229 *for $x_0 \geq A$. Moreover, the proportion can be calculated to be the scalar*

$$p^i = \ell \left(\mathbf{p}_0^i \circ \mathbf{r} \right) \quad (15)$$

230 *where ℓ is the left eigenvector of \mathbf{B}_0 corresponding to λ_1 with ℓ normalized by $\langle \ell^T, \mathbf{r} \rangle$.*

231 Theorem 3.3 provides a formula for the asymptotic proportion of neutral fractions based on the initial
 232 distribution at the leading edge of the population. The formula is simple because it depends only on the
 233 right and left eigenvectors of \mathbf{B}_0 and the initial proportion of neutral fractions. This theorem characterizes
 234 the fate of neutral fractions at the leading edge. One drawback to this theorem is that it is only valid
 235 for initial conditions that decay at a specific rate, $e^{-\frac{c-\mu}{\sigma^2}x}$, with a solution that moves at a specific speed,
 236 $c = c^*$. The reason why we cannot prove this theorem for $c > c^*$ and a slower decay rate for the initial

237 condition is because we do not have an explicit formula for the spreading speed $c > c^*$. For this proof, see
 238 Section 3.3.

239 It is also important to note that $A5''$ in Theorem 3.3 is not completely biologically realistic since the
 240 population grows without bound as $x \rightarrow -\infty$. However, this type of initial condition is needed based
 241 on the construction of our sub-solution and super-solutions. It may be possible to relax this assumption
 242 by studying the nonlinear operator and considering a more biologically realistic class of initial conditions.
 243 Next, we present the proofs of Theorems 3.1-3.3 in Section 3.3. For a comprehensive review of the necessary
 244 mathematical material needed in the proofs of the theorems, we direct the reader to Appendix B.

245 3.3 Proofs of the main theorems

246 *Proof of Theorem 3.1*

247 *Proof* For simplicity, we drop the superscript i in (4) and focus on a single neutral fraction. Our equation
 248 of interest is

$$\mathbf{v}_{t+1}(x) = \int_{-\infty}^{\infty} [\mathbf{K}(x-y) \circ \mathbf{B}(\mathbf{u}_t(y))] \mathbf{v}_t(y) dy. \quad (16)$$

249 Let

$$\mathbf{w}_0(x) = \frac{\mathbf{C}e^{-s_0(c)x}}{1+x^2} \quad (17)$$

250 where $\mathbf{C} = \kappa\phi$ and ϕ is the eigenvector of $\mathbf{H}(s_0(c))$ with dominant eigenvalue $\rho(s_0(c))$. From Lemma B.1,
 251 we know that $\mathbf{w}_0(x)$ is an upper bound for $\mathbf{v}_0(x)$. By Assumption A3, we know that $\mathbf{B}(\mathbf{u}_t(y))\mathbf{v} \leq \mathbf{B}_0\mathbf{v}$ for
 252 all $\mathbf{v} \geq 0$. Hence, we can construct a super-solution $\mathbf{w}_t(x)$ that satisfies the following equation

$$\mathbf{w}_{t+1}(x) = \int_{-\infty}^{\infty} [\mathbf{K}(x-y) \circ \mathbf{B}_0] \mathbf{w}_t(y) dy \quad (18)$$

253 with initial condition given by (17). By iterating we can write the solution to the above system as the t -fold
 254 convolution

$$\mathbf{w}_t(x) = [\mathbf{K}(x-y) \circ \mathbf{B}_0]^{*t} \mathbf{w}_0(y). \quad (19)$$

255 Applying the bilateral Laplace transform

$$\mathbf{W}_t(s) = [\mathbf{M}(s) \circ \mathbf{B}_0]^t \mathbf{W}_0(s) \quad (20)$$

$$= [\mathbf{H}(s)]^t \mathbf{W}_0(s). \quad (21)$$

256 Recall that $s_0(c)$ is the smallest positive root of $sc = \ln(\rho(s))$ for $c \geq c^*$. Then, the inverse transform as
 257 defined in Appendix B, see (130), yields

$$\mathbf{w}_t(x) = \frac{1}{2\pi i} \lim_{R \rightarrow \infty} \int_{s_0(c)-iR}^{s_0(c)+iR} [\mathbf{H}(s)]^t \mathbf{W}_0(s) e^{-sx} ds \quad (22)$$

$$= \frac{1}{2\pi} \int_{-\infty}^{\infty} [\mathbf{H}(s_0(c) + i\omega)]^t \mathbf{W}_0(s_0(c) + i\omega) e^{-(s_0(c)+i\omega)x} d\omega \quad (23)$$

258 for $c \geq c^*$. In the moving frame we have

$$\mathbf{w}_t(x_0 + ct) = \frac{1}{2\pi} \int_{-\infty}^{\infty} [\mathbf{H}(s_0(c) + i\omega)]^t \mathbf{W}_0(s_0(c) + i\omega) e^{-(s_0(c)+i\omega)x_0} e^{-(s_0(c)+i\omega)ct} d\omega. \quad (24)$$

259 Using the results from Lemma B.1, see Appendix B for details, we are able to write the initial condition in
 260 terms of a Fourier transform that is known. This is seen as follows,

$$\mathbf{W}_0(s_0(c) + i\omega) = \int_{-\infty}^{\infty} \mathbf{w}_0(x) e^{(s_0(c)+i\omega)x} dx \quad (25)$$

$$= \int_{-\infty}^{\infty} \mathbf{w}_0(x) e^{s_0(c)x} e^{i\omega x} dx \quad (26)$$

$$= \mathcal{F}[\mathbf{w}_0(x) e^{s_0(c)x}](-\omega) \quad (27)$$

$$= \mathbf{C}\pi e^{-|\omega|} \quad (28)$$

261 for all $\omega \in \mathbb{R}$. Recall that $\mathbf{C} = \kappa\phi$. This gives

$$\mathbf{w}_t(x_0 + ct) = \frac{1}{2\pi} \int_{-\infty}^{\infty} [\mathbf{H}(s_0(c) + i\omega)]^t \mathbf{C} \pi e^{-|\omega|} e^{-(s_0(c)+i\omega)x_0} e^{-(s_0(c)+i\omega)ct} d\omega \quad (29)$$

$$= \frac{1}{2} \int_{-\infty}^{\infty} [\mathbf{H}(s_0(c) + i\omega)]^t \kappa e^{-s_0(c)ct} \phi e^{-|\omega|} e^{-(s_0(c)+i\omega)x_0} e^{-i\omega ct} d\omega. \quad (30)$$

262 Since $s_0(c)c = \ln(\rho(s_0(c)))$, we have

$$\mathbf{w}_t(x_0 + ct) = \frac{\kappa e^{-s_0(c)x_0}}{2} \int_{-\infty}^{\infty} [\mathbf{H}(s_0(c) + i\omega)]^t e^{-\ln(\rho(s_0(c)))t} \phi e^{-|\omega|} e^{-i\omega x_0} e^{-i\omega ct} d\omega \quad (31)$$

$$= \frac{\kappa e^{-s_0(c)x_0}}{2} \int_{-\infty}^{\infty} [\mathbf{H}(s_0(c) + i\omega)]^t (\rho(s_0(c)))^{-t} \phi e^{-|\omega|} e^{-i\omega x_0} e^{-i\omega ct} d\omega. \quad (32)$$

263 Since $\rho(s_0(c))$ is the dominant eigenvalue of $\mathbf{H}(s_0(c))$ with eigenvector ϕ ,

$$\mathbf{w}_t(x_0 + ct) = \frac{\kappa e^{-s_0(c)x_0}}{2} \int_{-\infty}^{\infty} [\mathbf{H}(s_0(c) + i\omega)]^t [\mathbf{H}(s_0(c))]^{-t} \phi e^{-|\omega|} e^{-i\omega x_0} e^{-i\omega ct} d\omega. \quad (33)$$

264 Applying the matrix norm and using the sub-additive property, we find that

$$\|\mathbf{w}_t(x_0 + ct)\| \leq \frac{\kappa e^{-s_0(c)x_0}}{2} \int_{-\infty}^{\infty} \|[\mathbf{H}(s_0(c) + i\omega)]^t\| \|[\mathbf{H}(s_0(c))]^{-t}\| \|\phi\| e^{-|\omega|} |e^{-i\omega x_0}| |e^{-i\omega ct}| d\omega \quad (34)$$

$$= \frac{\kappa e^{-s_0(c)x_0}}{2} \int_{-\infty}^{\infty} \|[\mathbf{H}(s_0(c) + i\omega)]^t\| \|[\mathbf{H}(s_0(c))]^{-t}\| \|\phi\| e^{-|\omega|} d\omega. \quad (35)$$

265 We can also see that

$$|\mathbf{H}(s_0(c) + i\omega)| = |\mathbf{M}(s_0(c) + i\omega) \circ \mathbf{B}_0| \quad (36)$$

$$= \left| \int_{-\infty}^{\infty} [\mathbf{K}(x) \circ \mathbf{B}_0] e^{(s_0(c)+i\omega)x} dx \right| \quad (37)$$

$$= \left| \int_{-\infty}^{\infty} [\mathbf{K}(x) \circ \mathbf{B}_0] e^{s_0(c)x} (\cos(\omega x) + i \sin(\omega x)) dx \right| \quad (38)$$

$$= I, \quad (39)$$

266 where I is defined to be

$$I := \sqrt{\left(\int_{-\infty}^{\infty} [\mathbf{K}(x) \circ \mathbf{B}_0] e^{s_0(c)x} \cos(\omega x) dx \right)^2 + \left(\int_{-\infty}^{\infty} [\mathbf{K}(x) \circ \mathbf{B}_0] e^{s_0(c)x} \sin(\omega x) dx \right)^2}. \quad (40)$$

267 By the Cauchy-Schwarz inequality, using a similar technique as in Theorem 3 of (Marculis et al. 2017),

$$I < \int_{-\infty}^{\infty} [\mathbf{K}(x) \circ \mathbf{B}_0] e^{s_0(c)x} dx \quad (41)$$

$$= \mathbf{M}(s_0(c)) \circ \mathbf{B}_0 \quad (42)$$

$$= \mathbf{H}(s_0(c)) \quad (43)$$

268 for $\omega \neq 0$. From the above calculation we can conclude that $|\mathbf{H}(s_0(c) + i\omega)| < \mathbf{H}(s_0(c))$ for $\omega \neq 0$.

269 Consequently, $\rho(|\mathbf{H}(s_0(c) + i\omega)|) < \rho(s_0(c))$ for $\omega \neq 0$. By Gelfand's formula,

$$\lim_{t \rightarrow \infty} \|[\mathbf{H}(s_0(c) + i\omega)]^t\|^{\frac{1}{t}} = \rho(|\mathbf{H}(s_0(c) + i\omega)|) \quad \text{and} \quad (44)$$

$$\lim_{t \rightarrow \infty} \|[\mathbf{H}(s_0(c))]^{-t}\|^{\frac{1}{t}} = \frac{1}{\rho(s_0(c))}. \quad (45)$$

270 Thus, for $\omega \neq 0$, we can choose $\varepsilon > 0$ such that $(\rho(|\mathbf{H}(s_0(c) + i\omega)|) + \varepsilon) \left(\frac{1}{\rho(s_0(c))} + \varepsilon \right) < 1$. Therefore,

$$\|[\mathbf{H}(s_0(c) + i\omega)]^t\| \|[\mathbf{H}(s_0(c))]^{-t}\| < 1 \quad (46)$$

271 for large t and

$$\lim_{t \rightarrow \infty} \left\| \left\| [\mathbf{H}(s_0(c) + i\omega)]^t \right\| \left\| [\mathbf{H}(s_0(c))]^{-t} \right\| \right\| = 0. \quad (47)$$

272 From (35) and the dominated convergence theorem,

$$\lim_{t \rightarrow \infty} \|\mathbf{w}_t(x_0 + ct)\| \leq \frac{\kappa e^{-s_0(c)x_0}}{2} \int_{-\infty}^{\infty} \lim_{t \rightarrow \infty} \left\| \left\| [\mathbf{H}(s_0(c) + i\omega)]^t \right\| \left\| [\mathbf{H}(s_0(c))]^{-t} \right\| \|\phi\| e^{-|\omega|} d\omega \right. \quad (48)$$

$$\left. = \mathbf{0}. \quad (49)$$

273 Therefore, for any $A \in \mathbb{R}$ and $c \geq c^*$,

$$\lim_{t \rightarrow \infty} \max_{[A, \infty)} \mathbf{w}_t(x + ct) = \mathbf{0}. \quad (50)$$

274 Since \mathbf{w} was constructed as a super-solution, we can conclude that

$$\lim_{t \rightarrow \infty} \max_{[A, \infty)} \mathbf{v}_t(x + ct) = \mathbf{0}. \quad (51)$$

The proof of Theorem 3.1 is complete. \square

275 *Proof of Theorem 3.2*

276 *Proof* For simplicity, we focus on a single neutral fraction and drop the superscript i . By Assumption A3,
277 $\mathbf{B}(\mathbf{u}_t(y))\mathbf{v} \leq \mathbf{B}_0\mathbf{v}$ for all $\mathbf{v} \geq 0$, we can use a comparison principle to show that a new sequence $\mathbf{w}_t(x)$
278 defined by

$$\mathbf{w}_{t+1}(x) = \int_{-\infty}^{\infty} [\mathbf{K}(x-y) \circ \mathbf{B}_0] \mathbf{w}_t(y) dy \quad (52)$$

279 is always greater than the solution to any neutral fraction $\mathbf{v}_t(x)$ with the same initial condition, $\mathbf{w}_0(x) =$
280 $\mathbf{v}_0(x)$. By iterating we can write the solution to Equation (52) as the t -fold convolution

$$\mathbf{w}_t(x) = [\mathbf{K}(x-y) \circ \mathbf{B}_0]^{*t} \mathbf{w}_0(y). \quad (53)$$

281 Taking the bilateral Laplace transform

$$\mathcal{M}[\mathbf{w}_t(x)](s) = [\mathcal{M}[\mathbf{K}(x)](s) \circ \mathbf{B}_0]^t \mathcal{M}[\mathbf{w}_0(x)](s). \quad (54)$$

282 Since all of the dispersal kernels are Gaussian, we know that $\mathcal{M}[\mathbf{K}(x)](s) = e^{\frac{\sigma^2 s^2}{2} + \mu s} \mathbf{1}$ where $\mathbf{1}$ is a matrix
283 of all ones. Then,

$$[\mathcal{M}[\mathbf{K}(x)](s) \circ \mathbf{B}_0]^t \mathcal{M}[\mathbf{w}_0(x)](s) = \left[e^{\frac{\sigma^2 s^2}{2} + \mu s} \mathbf{1} \circ \mathbf{B}_0 \right]^t \mathcal{M}[\mathbf{w}_0(x)](s) \quad (55)$$

$$= \left[e^{\frac{\sigma^2 s^2}{2} + \mu s} \mathbf{B}_0 \right]^t \mathcal{M}[\mathbf{w}_0(x)](s) \quad (56)$$

$$= e^{\frac{\sigma^2 t s^2}{2} + \mu t s} [\mathbf{B}_0]^t \mathcal{M}[\mathbf{w}_0(x)](s) \quad (57)$$

$$= [\mathbf{B}_0]^t \mathcal{M} \left[\frac{1}{\sqrt{2\pi\sigma^2 t}} e^{-\frac{(x-\mu t)^2}{2\sigma^2 t}} \right] (s) \mathcal{M}[\mathbf{w}_0(x)](s) \quad (58)$$

$$= [\mathbf{B}_0]^t \mathcal{M}[(K_t * \mathbf{w}_0)(x)](s) \quad (59)$$

284 where K_t is $N(\mu t, \sigma^2 t)$. From (54)

$$\mathcal{M}[\mathbf{w}_t(x)](s) = [\mathbf{B}_0]^t \mathcal{M}[(K_t * \mathbf{w}_0)(x)](s). \quad (60)$$

285 Applying the inverse bilateral Laplace transform,

$$\mathbf{w}_t(x) = [\mathbf{B}_0]^t (K_t * \mathbf{w}_0)(x) \quad (61)$$

$$= [\mathbf{B}_0]^t \int_{-\infty}^{\infty} \frac{1}{\sqrt{2\pi\sigma^2 t}} e^{-\frac{(x-y-\mu t)^2}{2\sigma^2 t}} \mathbf{w}_0(y) dy \quad (62)$$

286 In the moving half-frame $[A + ct, \infty)$ with $c \geq c^*$ we have

$$\mathbf{w}_t(x_0 + ct) = [\mathbf{B}_0]^t \int_{-\infty}^{\infty} \frac{1}{\sqrt{2\pi\sigma^2 t}} e^{-\frac{(x_0+ct-y-\mu t)^2}{2\sigma^2 t}} \mathbf{w}_0(y) dy. \quad (63)$$

287 From (12), we know that $c^* = \sqrt{2\sigma^2 \ln(\lambda_1)} + \mu$, expanding the exponent, yields

$$\frac{(x_0 + ct - y - \mu t)^2}{2\sigma^2 t} = \frac{(x_0 - y)^2}{2\sigma^2 t} + \frac{2(c - \mu)t(x_0 - y) + (c - \mu)^2 t^2}{2\sigma^2 t} \quad (64)$$

$$\geq \frac{(x_0 - y)^2}{2\sigma^2 t} + \frac{c - \mu}{\sigma^2} (x_0 - y) + \ln(\lambda_1)t. \quad (65)$$

288 Thus,

$$\mathbf{w}_t(x_0 + ct) \leq \frac{[\mathbf{B}_0]^t}{\sqrt{2\pi\sigma^2 t}} \int_{-\infty}^{\infty} e^{-\frac{(x_0-y)^2}{2\sigma^2 t}} e^{-\frac{c-\mu}{\sigma^2}(x_0-y)} e^{-\ln(\lambda_1)t} \mathbf{w}_0(y) dy \quad (66)$$

$$= \left[\frac{\mathbf{B}_0}{\lambda_1} \right]^t \frac{1}{\sqrt{2\pi\sigma^2 t}} \int_{-\infty}^{\infty} e^{-\frac{(x_0-y)^2}{2\sigma^2 t}} e^{-\frac{c-\mu}{\sigma^2}(x_0-y)} \mathbf{w}_0(y) dy. \quad (67)$$

289 Since $x_0 \geq A$ and $e^{-\frac{(x_0-y)^2}{2\sigma^2 t}} \leq 1$, we have

$$\mathbf{w}_t(x_0 + ct) \leq \left[\frac{\mathbf{B}_0}{\lambda_1} \right]^t \frac{e^{-\frac{A(c-\mu)}{\sigma^2}}}{\sqrt{2\pi\sigma^2 t}} \int_{-\infty}^{\infty} e^{\frac{c-\mu}{\sigma^2} y} \mathbf{w}_0(y) dy. \quad (68)$$

290 From Lemma B.2, see Appendix B for details, we know that

$$\lim_{t \rightarrow \infty} \left[\frac{\mathbf{B}_0}{\lambda_1} \right]^t = \mathbf{r}\boldsymbol{\ell}, \quad (69)$$

where \mathbf{r} and $\boldsymbol{\ell}$ are the right and left eigenvectors of \mathbf{B}_0 corresponding to λ_1 respectively with $\boldsymbol{\ell}$ normalized by $\langle \boldsymbol{\ell}^T, \mathbf{r} \rangle$ to account for the scaling in \mathbf{r} . Note that $\mathbf{r}\boldsymbol{\ell}$ is a $m \times m$ matrix since \mathbf{r} is $m \times 1$ and $\boldsymbol{\ell}$ is $1 \times m$.

Thus since $\int_{-\infty}^{\infty} e^{\frac{c-\mu}{\sigma^2} y} \mathbf{w}_0(y) dy < \infty$ by Assumption A5' and (69) we have $\mathbf{w}_t(x_0 + ct) \rightarrow \mathbf{0}$ uniformly as $t \rightarrow \infty$ in $[A, \infty)$. Recall that $\mathbf{w}_t(x)$ was constructed as a super-solution, $\mathbf{0} \leq \mathbf{v}_t(x) \leq \mathbf{w}_t(x)$. This implies the uniform convergence of $\mathbf{v}_t(x) \rightarrow \mathbf{0}$ as $t \rightarrow \infty$ in the moving half-frame $[A + ct, \infty)$. The proof of Theorem 3.2 is complete. \square

291 *Proof of Theorem 3.3*

292 *Proof* For simplicity, we focus on a single neutral fraction and drop the superscript i . Using the fact that
293 $\mathbf{B}(\mathbf{u}_t(y))\mathbf{v} \leq \mathbf{B}_0\mathbf{v}$ for all $\mathbf{v} \geq 0$ we can use a comparison principle to show that a new sequence $\mathbf{w}_t(x)$
294 defined by

$$\mathbf{w}_{t+1}(x) = \int_{-\infty}^{\infty} [\mathbf{K}(x-y) \circ \mathbf{B}_0] \mathbf{w}_t(y) dy \quad (70)$$

295 is a super-solution to any neutral fraction $\mathbf{v}_t(x)$ with the same initial condition $\mathbf{w}_0(x) = \mathbf{v}_0(x)$. By iterating
296 we can write the solution to Equation (70) as the t -fold convolution

$$\mathbf{w}_t(x) = [\mathbf{K}(x-y) \circ \mathbf{B}_0]^{*t} \mathbf{w}_0(y). \quad (71)$$

297 Taking the bilateral Laplace transform

$$\mathcal{M}[\mathbf{w}_t(x)](s) = [\mathcal{M}[\mathbf{K}(x)](s) \circ \mathbf{B}_0]^t \mathcal{M}[\mathbf{w}_0(x)](s). \quad (72)$$

298 Since all of the dispersal kernels are Gaussian, we know that $\mathcal{M}[\mathbf{K}(x)](s) = e^{\frac{\sigma^2 s^2}{2} + \mu s} \mathbf{1}$ where $\mathbf{1}$ is a matrix
299 of all ones. Then, we can see that

$$[\mathcal{M}[\mathbf{K}(x)](s) \circ \mathbf{B}_0]^t \mathcal{M}[\mathbf{w}_0(x)](s) = \left[e^{\frac{\sigma^2 s^2}{2} + \mu s} \mathbf{1} \circ \mathbf{B}_0 \right]^t \mathcal{M}[\mathbf{w}_0(x)](s) \quad (73)$$

$$= \left[e^{\frac{\sigma^2 s^2}{2} + \mu s} \mathbf{B}_0 \right]^t \mathcal{M}[\mathbf{w}_0(x)](s) \quad (74)$$

$$= e^{\frac{\sigma^2 t s^2}{2} + \mu t s} \mathbf{I} [\mathbf{B}_0]^t \mathcal{M}[\mathbf{w}_0(x)](s) \quad (75)$$

$$= [\mathbf{B}_0]^t \mathcal{M} \left[\frac{1}{\sqrt{2\pi\sigma^2 t}} e^{-\frac{(x-\mu t)^2}{2\sigma^2 t}} \mathbf{I} \right] (s) \mathcal{M}[\mathbf{w}_0(x)](s) \quad (76)$$

$$= [\mathbf{B}_0]^t \mathcal{M} [(\mathbf{K}_t * \mathbf{w}_0)(x)](s) \quad (77)$$

300 where \mathbf{K}_t is a diagonal matrix with $N(\mu t, \sigma^2 t)$ entries and \mathbf{I} is the identity matrix. Thus, we have

$$\mathcal{M}[\mathbf{w}_t(x)](s) = [\mathbf{B}_0]^t \mathcal{M}[(\mathbf{K}_t * \mathbf{w}_0)(x)](s). \quad (78)$$

301 Then applying the inverse transform yields

$$\mathbf{w}_t(x) = [\mathbf{B}_0]^t (\mathbf{K}_t * \mathbf{w}_0)(x) \quad (79)$$

$$= [\mathbf{B}_0]^t \int_{-\infty}^{\infty} \frac{1}{\sqrt{2\pi\sigma^2 t}} e^{-\frac{(x-y-\mu t)^2}{2\sigma^2 t}} \mathbf{w}_0(y) dy \quad (80)$$

302 In the moving half-frame $[A + ct, \infty)$ with fixed $A \in \mathbb{R}$, consider the element $x_0 + ct$ with $c = c^* =$
 303 $\sqrt{2\sigma^2 \ln(\lambda_1)} + \mu$ where λ_1 is the dominant eigenvalue of \mathbf{B}_0 as given by (12). By rewriting $\mathbf{w}_t(x)$ in this
 304 moving half-frame we have

$$\mathbf{w}_t(x_0 + ct) = [\mathbf{B}_0]^t \int_{-\infty}^{\infty} \frac{1}{\sqrt{2\pi\sigma^2 t}} e^{-\frac{(x_0+ct-y-\mu t)^2}{2\sigma^2 t}} \mathbf{w}_0(y) dy. \quad (81)$$

305 Expanding the exponent, yields

$$\frac{(x_0 + ct - y - \mu t)^2}{2\sigma^2 t} = \frac{(y - x_0)^2}{2\sigma^2 t} + \frac{(c - \mu)(x_0 - y)}{\sigma^2} + \frac{(c - \mu)^2}{2\sigma^2} t. \quad (82)$$

306 Thus,

$$\mathbf{w}_t(x_0 + ct) = \frac{[\mathbf{B}_0]^t}{\sqrt{2\pi\sigma^2 t}} \int_{-\infty}^{\infty} e^{-\frac{(y-x_0)^2}{2\sigma^2 t}} e^{-\frac{(c-\mu)(x_0-y)}{\sigma^2}} e^{-\frac{(c-\mu)^2}{2\sigma^2} t} \mathbf{w}_0(y) dy \quad (83)$$

$$= \left[\frac{\mathbf{B}_0}{\lambda_1} \right]^t \frac{1}{\sqrt{2\pi\sigma^2 t}} \int_{-\infty}^{\infty} e^{-\frac{(y-x_0)^2}{2\sigma^2 t}} e^{-\frac{(c-\mu)(x_0-y)}{\sigma^2}} e^{\left[-\frac{(c-\mu)^2}{2\sigma^2} + \ln(\lambda_1) \right] t} \mathbf{w}_0(y) dy. \quad (84)$$

307 Since $c = c^* = \sqrt{2\sigma^2 \ln(\lambda_1)} + \mu$, we have that

$$\mathbf{w}_t(x_0 + ct) = \left[\frac{\mathbf{B}_0}{\lambda_1} \right]^t \frac{1}{\sqrt{2\pi\sigma^2 t}} \int_{-\infty}^{\infty} e^{-\frac{(y-x_0)^2}{2\sigma^2 t}} e^{-\frac{(c-\mu)(x_0-y)}{\sigma^2}} \mathbf{w}_0(y) dy. \quad (85)$$

308 From Assumption A5'', $\mathbf{w}_0(y) = (\mathbf{p}_0 \circ \mathbf{r}) e^{-\frac{c-\mu}{\sigma^2} y}$. Thus,

$$\mathbf{w}_t(x_0 + ct) = \left[\frac{\mathbf{B}_0}{\lambda_1} \right]^t (\mathbf{p}_0 \circ \mathbf{r}) e^{-\frac{(c-\mu)}{\sigma^2} x_0} \frac{1}{\sqrt{2\pi\sigma^2 t}} \int_{-\infty}^{\infty} e^{-\frac{(y-x_0)^2}{2\sigma^2 t}} dy \quad (86)$$

$$= \left[\frac{\mathbf{B}_0}{\lambda_1} \right]^t (\mathbf{p}_0 \circ \mathbf{r}) e^{-\frac{(c-\mu)}{\sigma^2} x_0}. \quad (87)$$

309 From Lemma B.2, see Appendix B for details, we know that

$$\lim_{t \rightarrow \infty} \left[\frac{\mathbf{B}_0}{\lambda_1} \right]^t = \mathbf{r} \boldsymbol{\ell} \quad (88)$$

310 where \mathbf{r} and $\boldsymbol{\ell}$ are the right and left eigenvectors of \mathbf{B}_0 corresponding to λ_1 respectively where $\boldsymbol{\ell}$ is normalized
 311 by $\langle \boldsymbol{\ell}^T, \mathbf{r} \rangle$. Thus,

$$\lim_{t \rightarrow \infty} \mathbf{w}_t(x_0 + ct) = \lim_{t \rightarrow \infty} \left[\frac{\mathbf{B}_0}{\lambda_1} \right]^t (\mathbf{p}_0 \circ \mathbf{r}) e^{-\frac{(c-\mu)}{\sigma^2} x_0} \quad (89)$$

$$= \mathbf{r} \boldsymbol{\ell} (\mathbf{p}_0 \circ \mathbf{r}) e^{-\frac{(c-\mu)}{\sigma^2} x_0} \quad (90)$$

$$= e^{-\frac{(c-\mu)}{\sigma^2} x_0} \mathbf{r} p. \quad (91)$$

312 From the above calculations, we find that the super-solution approaches a proportion, p , of the traveling
 313 wave for the linear equation where $p = \boldsymbol{\ell} (\mathbf{p}_0 \circ \mathbf{r})$. We now move onto our sub-solution. For any $0 < \varepsilon \ll 1$,
 314 $\boldsymbol{\delta}$ is chosen such that $(1 - \varepsilon) \mathbf{B}_0 \boldsymbol{\delta} = \mathbf{B}(\boldsymbol{\delta}) \boldsymbol{\delta}$ and we define

$$(\mathbf{B}_{sub}(\mathbf{u}; \varepsilon))_{jl} := \begin{cases} (1 - \varepsilon) (\mathbf{B}(\mathbf{u}))_{jl} & \text{if } (\mathbf{B}(\mathbf{u}))_{jl} \text{ is constant} \\ \beta_{jl}(\mathbf{u}; \varepsilon) & \text{if } (\mathbf{B}(\mathbf{u}))_{jl} \text{ is non-constant,} \end{cases} \quad (92)$$

315 where

$$\beta_{jt}(\mathbf{u}; \varepsilon) := \begin{cases} (1 - \varepsilon) (\mathbf{B}_0)_{jl} & \text{for } 0 \leq \mathbf{u} < \delta \\ (\mathbf{B}(\mathbf{u}))_{jl} & \text{for } \mathbf{u} \geq \delta. \end{cases} \quad (93)$$

316 Then,

$$\mathbf{z}_{t+1}(x) = \int_{-\infty}^{\infty} [\mathbf{K}(x - y) \circ \mathbf{B}_{sub}(\mathbf{u}_t(y); \varepsilon)] \mathbf{z}_t(y) dy \quad (94)$$

317 with $\mathbf{z}_0(x) = \mathbf{v}_0(x)$ is a sub-solution of $\mathbf{v}_t(x)$ by the comparison principle since $\mathbf{B}_{sub}(\mathbf{u}; \varepsilon)\mathbf{v} \leq \mathbf{B}(\mathbf{u})\mathbf{v}$ for
 318 all $\mathbf{v} \geq 0$. Define $c(\varepsilon) := \sqrt{2\sigma^2 \ln((1 - \varepsilon)\lambda_1)} + \mu$ where $(1 - \varepsilon)\lambda_1$ is the dominant eigenvalue of the constant
 319 matrix $(1 - \varepsilon)\mathbf{B}_0$. In the moving half-frame $[A + c(\varepsilon)t, \infty)$ with fixed $A \in \mathbb{R}$, choose x_0 large such that
 320 $\mathbf{u}_t(y)$ in (94) satisfies $\mathbf{u}_t(y) < \delta$ for all t where $y \in [x_0 + c(\varepsilon)t, \infty)$. Then by the definition of $\mathbf{B}_{sub}(\mathbf{u}; \varepsilon)$

$$\mathbf{z}_{t+1}(x_0 + c(\varepsilon)t) = \int_{-\infty}^{\infty} [\mathbf{K}(x_0 + c(\varepsilon)t - y) \circ (1 - \varepsilon)\mathbf{B}_0] \mathbf{z}_t(y) dy. \quad (95)$$

321 By iterating we can write the solution to (95) as the t -fold convolution

$$\mathbf{z}_t(x_0 + c(\varepsilon)t) = [\mathbf{K}(x_0 + c(\varepsilon)t - y) \circ (1 - \varepsilon)\mathbf{B}_0]^{*t} \mathbf{z}_0(y). \quad (96)$$

322 Since we assumed that all of the dispersal kernels are Gaussian, by repeating calculations done previously
 323 we find that

$$\mathbf{z}_t(x_0 + c(\varepsilon)t) = [(1 - \varepsilon)\mathbf{B}_0]^t \int_{-\infty}^{\infty} \frac{1}{\sqrt{2\pi\sigma^2 t}} e^{-\frac{(x_0 + c(\varepsilon)t - y - \mu t)^2}{2\sigma^2 t}} \mathbf{z}_0(y) dy \quad (97)$$

$$= \frac{[(1 - \varepsilon)\mathbf{B}_0]^t}{\sqrt{2\pi\sigma^2 t}} \int_{-\infty}^{\infty} e^{-\frac{(x_0 - y)^2}{2\sigma^2 t}} e^{-\frac{(c(\varepsilon) - \mu)(x_0 - y)}{\sigma^2}} e^{-\frac{(c(\varepsilon) - \mu)^2}{2\sigma^2} t} \mathbf{z}_0(y) dy \quad (98)$$

$$= \left[\frac{(1 - \varepsilon)\mathbf{B}_0}{(1 - \varepsilon)\lambda_1} \right]^t \frac{1}{\sqrt{2\pi\sigma^2 t}} \int_{-\infty}^{\infty} e^{-\frac{(x_0 - y)^2}{2\sigma^2 t}} e^{-\frac{(c(\varepsilon) - \mu)(x_0 - y)}{\sigma^2}} e^{\left[-\frac{(c(\varepsilon) - \mu)^2}{2\sigma^2} + \ln((1 - \varepsilon)\lambda_1) \right] t} \mathbf{z}_0(y) dy \quad (99)$$

$$= \left[\frac{\mathbf{B}_0}{\lambda_1} \right]^t \frac{1}{\sqrt{2\pi\sigma^2 t}} \int_{-\infty}^{\infty} e^{-\frac{(x_0 - y)^2}{2\sigma^2 t}} e^{-\frac{(c(\varepsilon) - \mu)(x_0 - y)}{\sigma^2}} e^{\left[-\frac{(c(\varepsilon) - \mu)^2}{2\sigma^2} + \ln((1 - \varepsilon)\lambda_1) \right] t} \mathbf{z}_0(y) dy. \quad (100)$$

324 Since $c(\varepsilon) = \sqrt{2\sigma^2 \ln((1 - \varepsilon)\lambda_1)} + \mu$,

$$\mathbf{z}_t(x_0 + c(\varepsilon)t) = \left[\frac{\mathbf{B}_0}{\lambda_1} \right]^t \frac{1}{\sqrt{2\pi\sigma^2 t}} \int_{-\infty}^{\infty} e^{-\frac{(x_0 - y)^2}{2\sigma^2 t}} e^{-\frac{(c(\varepsilon) - \mu)(x_0 - y)}{\sigma^2}} \mathbf{z}_0(y) dy. \quad (101)$$

325 Note that the integrand in (101) is nonnegative and integrable. Using Fatou's lemma we fix t and let $\varepsilon \rightarrow 0$,
 326 giving

$$\mathbf{z}_t(x_0 + ct) = \liminf_{\varepsilon \rightarrow 0} \mathbf{z}_t(x_0 + c(\varepsilon)t) \quad (102)$$

$$= \liminf_{\varepsilon \rightarrow 0} \left[\frac{\mathbf{B}_0}{\lambda_1} \right]^t \frac{1}{\sqrt{2\pi\sigma^2 t}} \int_{-\infty}^{\infty} e^{-\frac{(x_0 - y)^2}{2\sigma^2 t}} e^{-\frac{(c(\varepsilon) - \mu)(x_0 - y)}{\sigma^2}} \mathbf{z}_0(y) dy \quad (103)$$

$$\geq \left[\frac{\mathbf{B}_0}{\lambda_1} \right]^t \frac{1}{\sqrt{2\pi\sigma^2 t}} \int_{-\infty}^{\infty} \liminf_{\varepsilon \rightarrow 0} e^{-\frac{(x_0 - y)^2}{2\sigma^2 t}} e^{-\frac{(c(\varepsilon) - \mu)(x_0 - y)}{\sigma^2}} \mathbf{z}_0(y) dy \quad (104)$$

$$= \left[\frac{\mathbf{B}_0}{\lambda_1} \right]^t \frac{1}{\sqrt{2\pi\sigma^2 t}} \int_{-\infty}^{\infty} e^{-\frac{(x_0 - y)^2}{2\sigma^2 t}} e^{-\frac{(c - \mu)(x_0 - y)}{\sigma^2}} \mathbf{z}_0(y) dy. \quad (105)$$

327 From Assumption A5'', $\mathbf{z}_0(y) = (\mathbf{p}_0 \circ \mathbf{r}) e^{-\frac{(c - \mu)}{\sigma^2} y}$. Thus, by the same calculations used in (86)-(87) for the
 328 super-solution

$$\mathbf{z}_t(x_0 + ct) \geq \left[\frac{\mathbf{B}_0}{\lambda_1} \right]^t (\mathbf{p}_0 \circ \mathbf{r}) e^{-\frac{(c - \mu)}{\sigma^2} x_0}. \quad (106)$$

329 From Lemma B.2, see Appendix B for details, we see that

$$\lim_{t \rightarrow \infty} \left[\frac{\mathbf{B}_0}{\lambda_1} \right]^t = \mathbf{r}\ell, \quad (107)$$

330 where \mathbf{r} and $\boldsymbol{\ell}$ are the right and left eigenvectors corresponding to λ_1 respectively where the $\boldsymbol{\ell}$ is normalized
 331 by $\langle \boldsymbol{\ell}^T, \mathbf{r} \rangle$. Thus,

$$\lim_{t \rightarrow \infty} \mathbf{z}_t(x_0 + ct) \geq \lim_{t \rightarrow \infty} \left[\frac{\mathbf{B}_0}{\lambda_1} \right]^t (\mathbf{p}_0 \circ \mathbf{r}) e^{-\frac{(c-\mu)}{\sigma^2} x_0} \quad (108)$$

$$= \mathbf{r} \boldsymbol{\ell} (\mathbf{p}_0 \circ \mathbf{r}) e^{-\frac{(c-\mu)}{\sigma^2} x_0} \quad (109)$$

$$= e^{-\frac{(c-\mu)}{\sigma^2} x_0} \mathbf{r} p. \quad (110)$$

332 Asymptotically, our sub-solution is bounded below by a proportion of the traveling wave for the linear
 333 equation where $p = \boldsymbol{\ell} (\mathbf{p}_0 \circ \mathbf{r})$. Since our super-solution satisfies

$$\lim_{t \rightarrow \infty} \mathbf{w}_t(x_0 + ct) \leq e^{-\frac{(c-\mu)}{\sigma^2} x_0} \mathbf{r} p, \quad (111)$$

334 and our sub-solution satisfies

$$\lim_{t \rightarrow \infty} \mathbf{z}_t(x_0 + ct) \geq e^{-\frac{(c-\mu)}{\sigma^2} x_0} \mathbf{r} p \quad (112)$$

335 it follows that

$$\lim_{t \rightarrow \infty} \mathbf{v}_t(x_0 + ct) = e^{-\frac{(c-\mu)}{\sigma^2} x_0} \mathbf{r} p. \quad (113)$$

The proof of Theorem 3.3 is complete. \square

336 4 Numerical simulations

337 In this section, we illustrate the theory of Section 3 with a numerical example. All simulations were done
 338 using the fast Fourier transform technique (Cooley and Tukey 1965). This method is better than classical
 339 quadrature because it speeds up the numerical process from $O(n^2)$ to $O(n \log(n))$.

340 We begin with a two-stage population model of juveniles, J , and adults, A . The equations in this model
 341 are given below,

$$\begin{aligned} J_{t+1}^i(x) &= \int_{-\infty}^{\infty} k(x-y) \zeta (1-m) J_t^i(y) dy + \int_{-\infty}^{\infty} k(x-y) f_0 e^{-\sum_{i=1}^n (J_t^i(y) + A_t^i(y))} A_t^i(y) dy, \\ A_{t+1}^i(x) &= \int_{-\infty}^{\infty} k(x-y) \zeta m J_t^i(y) dy + \int_{-\infty}^{\infty} k(x-y) \zeta A_t^i(y) dy, \end{aligned} \quad (114)$$

342 where

$$k(x-y) = \frac{1}{\sqrt{2\pi\sigma^2}} e^{-\frac{(x-y)^2}{2\sigma^2}}. \quad (115)$$

343 The demography in (114) follows a classical model for biological invasions (Neubert and Caswell 2000), but
 344 we assume Gaussian dispersal to align with the assumptions in our theorems. In (114), ζ is the probability
 345 of survival to the next generation, m is the probability of maturation from a juvenile to an adult, f_0 is the
 346 number of juveniles produced by an adult in the absence of density-dependent effects. All individuals are
 347 assumed to disperse according to a Gaussian dispersal kernel. The growth function for adults producing
 348 juveniles is assumed to be a Ricker type growth function where the nonlinearity depends on the density of
 349 both juveniles and adults. In the juvenile equation of (114), juveniles can remain juveniles if they survive
 350 and do not mature and adults from location y can produce juveniles that disperse to location x . In the
 351 adult equation of (114), juveniles become adults if they survive and mature, and adults remain adults if
 352 they survive from the previous year.

353 Let

$$\mathbf{v}_t^i(x) = \begin{bmatrix} J_t^i(x) \\ A_t^i(x) \end{bmatrix}, \quad (116)$$

$$\mathbf{K}(x-y) = \begin{bmatrix} \frac{1}{\sqrt{2\pi\sigma^2}} e^{-\frac{(x-y)^2}{2\sigma^2}} & \frac{1}{\sqrt{2\pi\sigma^2}} e^{-\frac{(x-y)^2}{2\sigma^2}} \\ \frac{1}{\sqrt{2\pi\sigma^2}} e^{-\frac{(x-y)^2}{2\sigma^2}} & \frac{1}{\sqrt{2\pi\sigma^2}} e^{-\frac{(x-y)^2}{2\sigma^2}} \end{bmatrix}, \text{ and} \quad (117)$$

$$\mathbf{B}(\mathbf{u}_t(y)) = \begin{bmatrix} \zeta(1-m) f_0 e^{-\sum_{i=1}^n (J_t^i(y) + A_t^i(y))} \\ \zeta m & \zeta \end{bmatrix}. \quad (118)$$

354 Then we can write (114) in the matrix and vector notation provided in (4).

355 First, let us verify that the assumptions of Theorems 3.2 and 3.3 are satisfied. Recall that Assumptions
 356 A1-A3 and A4' are the same for these two theorems. For Assumption A1, it is clear that our population
 357 projection matrix, $\mathbf{B}(\mathbf{u}_t(y))$, is nonnegative from (118) since $\zeta, m, f_0 > 0$. We can calculate \mathbf{B}_0 to be

$$\mathbf{B}_0 = \begin{bmatrix} \zeta(1-m) & f_0 \\ \zeta m & \zeta \end{bmatrix}. \quad (119)$$

358 Thus, \mathbf{B}_0 is primitive. For Assumption A2, the dominant eigenvalue of \mathbf{B}_0 is greater than one if

$$f_0 > \frac{(1-\zeta)(1-\zeta(1-m))}{\zeta m}. \quad (120)$$

359 For details of this calculation see Proposition 3.1 of Marculis and Lui (2016). Since $e^{-\sum_{i=1}^n (J_i^i(y) + A_i^i(y))} \leq 1$
 360 we have $\mathbf{B}(\mathbf{u}_t(y))\mathbf{v} \leq \mathbf{B}_0\mathbf{v}$ for all $\mathbf{v} \geq 0$ and Assumption A3 is satisfied. Even though our operator is not
 361 order preserving because of the overcompensation in the Ricker function, Proposition 3.1 in Li et al. (2009)
 362 suggests that the calculation for the spreading speed should still hold true. Assumption A4' is clear from
 363 the definition of (117). Finally, if we assume our initial condition to decay faster than $e^{-\frac{c-\mu}{\sigma^2}x}$, then the
 364 neutral fractions will satisfy Assumption A5' of Theorem 3.2 and we can see that (114) has a unique positive
 365 steady state given by

$$J^* = \frac{1-\zeta}{\zeta m} A^* \text{ and } A^* = -\ln\left(\frac{(1-\zeta)(1-\zeta(1-m))}{f_0 \zeta m}\right), \quad (121)$$

366 see again Proposition 3.1 of Marculis and Lui (2016). In our numerical simulations the only neutral fraction
 367 that does not decay faster than $e^{-\frac{c-\mu}{\sigma^2}x}$ is the one at the leading edge because it was chosen to have an
 368 initial form of the traveling wave solution with $c = c^*$. It should be mentioned here that since we are
 369 solving this problem numerically it is solved on a finite domain and this is only an approximation to the
 370 solution. Therefore, in the moving half-frame, the only neutral fractions that we see are the ones initially
 371 at the leading edge. The neutral fractions at the leading edge do not satisfy the exact Assumption A5'' of
 372 Theorem 3.3, but asymptotically they decay like $e^{-\frac{c-\mu}{\sigma^2}x}$. However, the asymptotic proportion calculated
 373 from Theorem 3.3 agrees with the numerical simulation suggesting that this result should be able to extend
 374 to a wider array of initial conditions.

375 We provide some numerical simulations to see the neutral genetic patterns produced by (114). We begin
 376 by running a simulation where the juvenile and adult populations have the same initial distribution as seen
 377 in Figure 1(a). This simulation shows that the spread of both juveniles and adults is dominated by the
 378 neutral fraction at the leading edge as seen in Figure 1(b). Switching the ordering of the neutral fractions
 379 behind the leading edge does not affect the asymptotic behavior in the moving frame. This observation is
 380 consistent with the founder effect. The simulations seen in Figure 1 agree with the results of Theorems 3.2
 381 and 3.3.

382 For our next simulation, we consider the case where the distribution of the neutral fractions of juveniles
 383 and adults do not appear in the same order. This is seen in Figure 2(a). Here we keep the same initial
 384 distribution of juvenile individuals as in Figure 1(a), but the initial distribution of adult neutral fractions
 385 is assorted differently. In Figure 2(a) we can see that initially the neutral fractions at the leading edge of
 386 the juvenile and adult populations are light gray and red respectively. Figure 2(b) shows the distribution of
 387 neutral fractions at $t = 100$. At the leading edge the spread is dominated by the light gray and red neutral
 388 fractions. This simulation agrees with our theoretical results because Theorem 3.2 and 3.3 suggest that the
 389 spread should be dominated by the neutral fractions that are initially at the leading edge of the population.
 390 Again we see that the neutral fractions behind the leading edge do not contribute to the asymptotic spread.

391 5 Discussion

392 The main objective of this work is to understand the effect that stage-structure has on the neutral genetic
 393 composition of expanding populations as outlined in Section 1. We derived the model for the inside dyna-
 394 mics of a stage-structured integrodifference equation in Section 2.1. Section 2.2 describes five of our main
 395 assumptions related to demography and dispersal. Four of these assumptions are related to the population
 396 projection matrix and the fifth is related to the form of the dispersal kernel.

397 The three main results of the paper are provided in Section 3, with their respective proofs in Section 3.3.
 398 Theorem 3.1 is our first main result, which provides sufficient conditions for a neutral fraction to converge

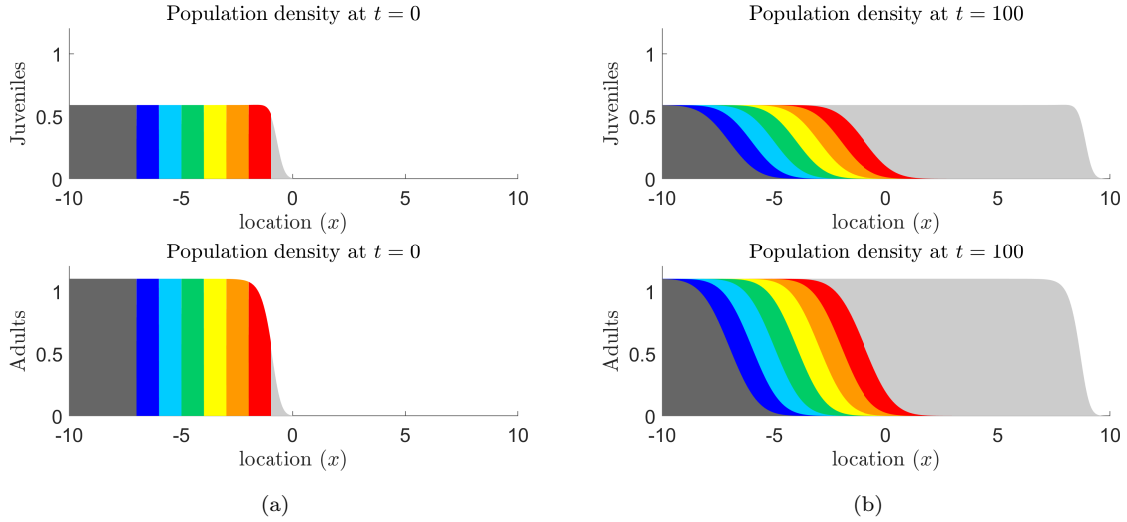


Fig. 1 Numerical realization of (114) for the parameter values $\sigma^2 = 0.01$, $\mu = 0$, $\zeta = 0.7$, $m = 0.8$, and $f_0 = 2.5$ for $n = 8$ neutral fractions. In (a) the plots are the initial conditions for the juvenile and adult populations. Notice that the distribution of neutral fractions for juvenile and adult populations have the same order. In (b) we plot the densities of the juvenile and adult neutral fractions at $t = 100$.

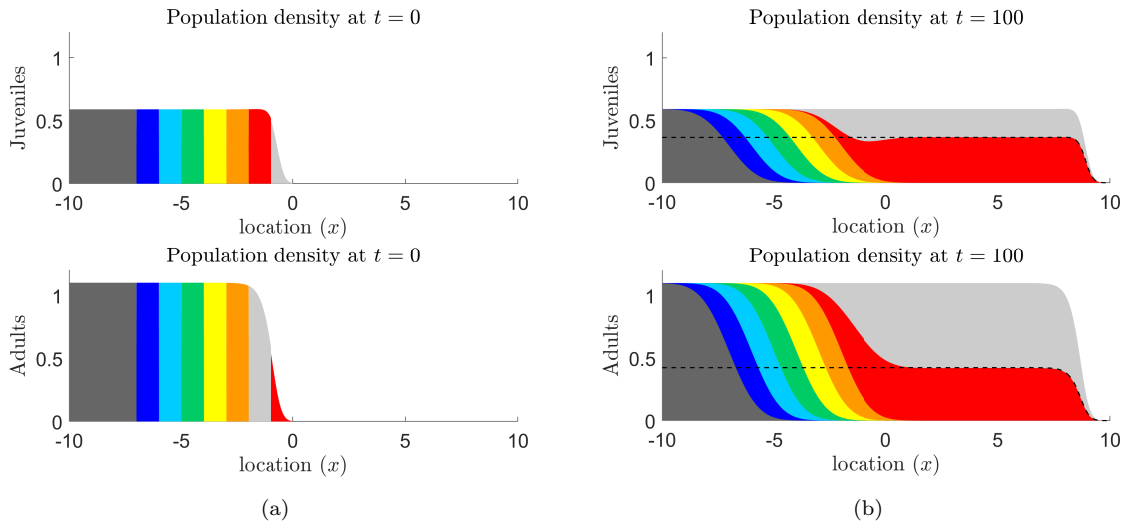


Fig. 2 Numerical realization of (114) for the parameter values $\sigma^2 = 0.01$, $\mu = 0$, $\zeta = 0.7$, $m = 0.8$, and $f_0 = 2.5$ for $n = 8$ neutral fractions. For these parameters $\mathbf{u}^* = (J^*, A^*) = (0.5900, 1.1013)$. In (a) the plots are the initial conditions for the juvenile and adult population. Notice that the distribution of the first two neutral fractions is different for juveniles and adults. The plots in (b) are the densities of the juvenile and adult neutral fractions at $t = 100$. The neutral genetic pattern produced here is due to the difference in the initial distribution of neutral fractions for juveniles and adults. The dashed lines in (b) are calculated from Theorem 3.3, they represent the proportions of red juveniles and adults. Behind the leading edge the proportions are $p^2 J^* = 0.3629$ for juveniles and $p^1 A^* = 0.4238$ for adults.

399 uniformly to zero in the moving half-frame. The five assumptions that must be satisfied are as follows: the
400 population projection matrix must be nonnegative, the population projection matrix evaluated at zero must
401 be primitive and its dominant eigenvalue must be greater than one, the population projection matrix must
402 be maximal at the trivial steady state, all dispersal kernels must be thin-tailed, and the initial condition
403 must satisfy the decay assumption given in Lemma B.1. It should be noted that the Dirac delta function
404 is a thin-tailed dispersal kernel and thus we can consider cases where there is no dispersal between some
405 transitions making this theorem very general in terms of the dispersal assumptions.

406 The second main result is Theorem 3.2. Similar to Theorem 3.1, this theorem also shows conditions
407 under which each neutral fraction converges uniformly to zero in the moving half-frame. The difference
408 with this theorem is that we make a stronger assumption on the dispersal kernels in exchange for a weaker
409 condition on the initial condition. In particular, we assume that all dispersal kernels are Gaussian with
410 identical means and variances. Due to this assumption, we are then able to relax the decay condition on
411 the initial condition of the population to be slightly weaker than is required for Theorem 3.1. The proof
412 for Theorem 3.2 is more elegant than the proof for Theorem 3.1. However, this comes at some cost in the
413 biological realism of the model since it is not common for all stages and transitions to disperse exactly via
414 a Gaussian distribution.

415 The final result is given in Theorem 3.3. The first four assumptions of this theorem are the same as
416 Theorem 3.2. The fifth assumption assumes that the initial condition decays according to the traveling
417 wave ansatz for the linear equation. Under these assumptions, we are able to asymptotically calculate the
418 proportion that each neutral fraction approaches in the moving frame. This proportion is dependent on the
419 right and left eigenvectors of the population projection matrix evaluated at zero and the initial proportion
420 of each neutral fraction at the leading edge. The proof relies on the construction of super- and sub-solutions
421 to the system. The super-solution, as expected, is chosen to be the linearization of our operator while the
422 sub-solution is defined in a piecewise manner to lie below the nonlinearities. Since all dispersal kernels were
423 assumed to be identical Gaussian distributions, the proportion calculated by Theorem 3.3 does not apply
424 when some stages and transitions do not disperse in the same way.

425 After completion of the mathematical results, we performed some numerical simulations in Section 4
426 to compare our analytical results to a reasonable biological model. We chose to look at a classical two-
427 stage juvenile adult model where dispersal occurs between all stages and transitions. The first simulation,
428 in Figure 1, shows that the spread is dominated by the neutral fraction at the leading edge which is an
429 extreme version of the founder effect. However, since we are working with a system of equations, it is
430 possible for the initial distribution of neutral fractions in the juvenile and adult stages to be different. This
431 is seen in Figure 2(a). As predicted from Theorem 3.2, in Figure 2(b), we see that all neutral fractions,
432 except the ones at the leading edge of the juvenile and adult populations, converge uniformly to zero in
433 the moving half-frame. The asymptotic proportions for the two neutral fractions that were initially at the
434 leading edge of the juvenile and adult populations are given by the formula in Theorem 3.3 and plotted as
435 the dashed line in Figure 2(b).

436 As expected, some of the same results obtained here are similar to those for the scalar population
437 model. That is, Theorem 3.1 and Theorem 3.2 are equivalent to their scalar counterparts, Theorem 3 and
438 Theorem 1 respectively, given in Marculis et al. (2017). However, Theorem 3.3 provides a new result for a
439 special case of interacting neutral fractions at the leading edge. This is not possible in the scalar population
440 model. From this theorem, we see the ability for multiple neutral fractions to contribute to the spread of
441 the population. Contributions from multiple neutral fractions to the population spread are only possible
442 in the scalar model when there is a strong Allee effect (Marculis et al. 2017). Although we would expect
443 similar behavior from our stage-structured model, we are not able to analyze the inside dynamics of a
444 stage-structured model with a strong Allee effect. This is due to the requirement that our results for the
445 strong Allee effect in scalar systems rely on the operator being compact. For a system of equations the
446 necessary theory is more complicated and we were unable to perform this analysis. In the special case
447 where all dispersal kernels are Gaussian with the same mean and variance and all entries of the population
448 projection matrix have the same strong Allee effect type per-capita growth function, then Theorem 2 given
449 in Marculis et al. (2017) can be applied. However, such stringent assumptions would defeat the purpose for
450 considering a stage-structured population model because all stages and transitions would grow and disperse
451 in the same way, essentially reducing the stage-structured model to a scalar equation.

452 The interesting additional feature that the stage-structured population model offers over scalar models
453 is the ability to have a different initial distribution of neutral fractions for each stage. This difference can
454 lead to multiple neutral fractions driving the spread of the population. Here, we see these dynamics solely
455 for the reason that the initial spatial distribution of neutral fractions is different for each stage.

456 Several assumptions about the integrodifference dynamics and dispersal kernels limit the applicability
457 of the results in this paper. One limitation to the applicability of our work is seen in Assumption A3.
458 Here we require that our population projection matrix is maximal at zero. This means that we are not
459 considering any kind of demography with Allee effects. In order to prove the asymptotic proportion result
460 seen in Theorem 3.3 we make some restrictive assumptions on the dispersal kernels and initial conditions
461 in the model. Assumption A4' in Theorem 3.3 states that all dispersal kernels are Gaussian with the same
462 mean and variance. This assumption may be unrealistic for many populations because the reason to use a
463 stage-structured population model over a scalar population model is to include differences in demography

464 and dispersal between stages. Assumption $A5''$ in Theorem 3.3 makes the assumption that the initial
465 conditions are in the form of the traveling wave ansatz for the linear equation. It would be beneficial
466 to generalize Theorem 3.3 for initial conditions that are in the form of the traveling wave solution. The
467 numerical simulations show that we should be able to relax our sixth assumption in our in theorems to a
468 more general class of initial conditions. These simulations are not only useful for verifying our mathematical
469 results, but they also provide some insight into opportunities for further mathematical analysis.

470 A Asymptotic speed of propagation for a system

471 The following Proposition is taken from (Lui 1989a). Let $\beta \in \mathbb{R}^n$ be a positive vector. We define

$$C = \{\mathbf{u} = (u^1, \dots, u^n) \mid \mathbf{0} \leq \mathbf{u}(x) \leq \beta, u^i(x) : \mathbb{R} \rightarrow [0, \beta^i] \\ \text{is piecewise continuous for } i = 1, \dots, n\}.$$

472 The operator \mathbf{Q} used in our analytical results is given by

$$\mathbf{Q}[\mathbf{u}] = \int_{-\infty}^{\infty} [\mathbf{K}(x-y) \circ \mathbf{B}(\mathbf{u}(y))] \mathbf{u}(y) dy. \quad (122)$$

473 **Proposition A.1** Let $\mathbf{Q} = (Q^1, \dots, Q^n) : C \rightarrow C$ satisfy the following conditions:

- 474 (1) $\mathbf{Q}[\mathbf{0}] = \mathbf{0}$, $\mathbf{Q}[\beta] = \beta$, $\mathbf{0}$ is unstable and β is stable with respect to \mathbf{Q} .
475 (2) \mathbf{Q} is translation invariant and has no other fixed-point besides $\mathbf{0}$ and β in C .
476 (3) \mathbf{Q} is monotone or order-preserving in C ; that is, if $\mathbf{u} \leq \mathbf{v}$ in C , then $\mathbf{Q}[\mathbf{u}] \leq \mathbf{Q}[\mathbf{v}]$.
477 (4) \mathbf{Q} is continuous in the topology of uniform convergence on bounded subsets of \mathbb{R} .
478 (5) Let

$$(\mathbf{M}[\mathbf{u}](x))_i = \sum_{j=1}^n \int_{-\infty}^{\infty} \mathbf{u}_j(x-y) m^{ij}(y) dy. \quad (123)$$

479 be the linearization of \mathbf{Q} at $\mathbf{0}$, where $m^{ij}(y) \geq 0$ is an integrable function. We assume that

$$\mathbf{Q}[\mathbf{u}] \leq \mathbf{M}[\mathbf{u}] \quad \text{for all } \mathbf{u} \in C. \quad (124)$$

480 (6) The matrix $\mathbf{B}(s) = (b^{ij}(s))$, where

$$b^{ij}(s) = \int_{-\infty}^{\infty} e^{sy} m^{ij}(y) dy \quad (125)$$

481 is irreducible for $0 < s < s^+$.

482 Let $\rho(s)$ be the dominant eigenvalue of $\mathbf{B}(s)$ and let

$$c^* = \min_{0 < s < s^+} \frac{1}{s} \ln \rho(s). \quad (126)$$

483 Then c^* is the asymptotic speed of propagation of the operator \mathbf{Q} in the positive direction in the following sense. Let $\mathbf{u}_0 \in C$,
484 \mathbf{u}_0 is non-trivial and vanishes outside of a bounded interval in \mathbb{R} . Let \mathbf{u}_t be defined by $\mathbf{u}_{t+1} = \mathbf{Q}[\mathbf{u}_t]$ for $t = 0, 1, 2, \dots$
485 Then for any small $\varepsilon > 0$,

$$\lim_{t \rightarrow \infty} \min_{x \leq t(c^* - \varepsilon)} |\mathbf{u}_t(x) - \beta| = 0 \quad (127)$$

$$\text{and} \quad \lim_{t \rightarrow \infty} \max_{x \geq t(c^* + \varepsilon)} |\mathbf{u}_t(x)| = 0. \quad (128)$$

486 B Mathematical details

487 The purpose of this section is to provide the mathematical background needed to prove the theorems in Section 3. One
488 tool that is used throughout all of our theorems is the reflected Bilateral Laplace transform.

489 **Definition 2** Let $f : \mathbb{R} \rightarrow \mathbb{R}$ where f is piecewise continuous on every finite interval in \mathbb{R} and there exists a $M \in \mathbb{R}^+$
490 such that $|f(x)| \leq M e^{-sx}$ for all $x \in \mathbb{R}$ and $0 < s < s^+$. Then, the reflected bilateral Laplace transform and its inverse
491 are defined to be

$$F(s) = \mathcal{M}[f(x)] := \int_{-\infty}^{\infty} f(x) e^{sx} dx, \quad \text{and} \quad (129)$$

$$f(x) = \mathcal{M}^{-1}[F(s)] := \frac{1}{2\pi i} \lim_{R \rightarrow \infty} \int_{\gamma - iR}^{\gamma + iR} F(s) e^{-sx} ds \quad (130)$$

492 for $0 < s < s^+$, where the integration in Equation (130) is over the vertical line, $\text{Re}(s) = \gamma$ in the complex plane and γ is
493 greater than the real parts of all singularities of $F(s)$.

494 By using the convolution theorem, the reflected bilateral Laplace transform can be used to write the solution to our
 495 model in terms of the initial condition. This theorem states that the reflected bilateral Laplace transform of a convolution
 496 is the product of the reflected bilateral Laplace transforms. That is,

$$\mathcal{M}[f(x) * h(x)](s) = F(s)H(s). \quad (131)$$

497 Note that the reflected bilateral Laplace transform of a probability density function is also referred to as its moment
 498 generating function.

499 Next, we provide results regarding vector and matrix analysis that are relevant to our subsequent analysis. First, it
 500 should be noted that when we write $\mathbf{x} \geq \mathbf{y}$, the inequality is element-wise. That is, $x_i \geq y_i$ for each i . In a similar manner,
 501 $\mathbf{x} > \mathbf{y}$ means that $x_i > y_i$ for each i . For the matrix analysis, the following definitions and proposition are needed:

502 **Definition 3** Let $\lambda_1, \dots, \lambda_m$ be the eigenvalues of a matrix \mathbf{A} . Then its spectral radius $\rho(\mathbf{A})$ is defined as:

$$\rho(\mathbf{A}) := \max_{i=1, \dots, m} |\lambda_i|. \quad (132)$$

503 In other words, the spectral radius of a matrix \mathbf{A} is the modulus of the largest eigenvalue.

504 **Definition 4** A matrix \mathbf{A} is called nonnegative, $\mathbf{A} \geq \mathbf{0}$, if $a_{ij} \geq 0$ for all i, j .

505 Definition 4 states that a matrix is nonnegative if all elements of the matrix are greater than or equal to zero. Next, we
 506 consider primitive matrices.

507 **Definition 5** A nonnegative matrix \mathbf{A} is primitive if there is a positive integer k such that $\mathbf{A}^k > \mathbf{0}$.

508 Another important concept is that of the dominant eigenvalue of a matrix.

509 **Definition 6** Let $\lambda_1, \dots, \lambda_m$ be the eigenvalues of an $m \times m$ matrix \mathbf{A} . If $|\lambda_1| > |\lambda_j|$ for $j = 2, \dots, m$, then λ_1 is called
 510 the dominant eigenvalue of \mathbf{A} .

511 Next, we discuss the Perron-Frobenius theorem for nonnegative primitive matrices (Bapat and Raghavan 1997).

512 **Proposition B.1 (Perron-Frobenius theorem)** Let $\mathbf{A} \geq \mathbf{0}$ be an $m \times m$ primitive matrix. Then $\mathbf{A}\mathbf{y} = \lambda_1\mathbf{y}$ for some
 513 $\lambda_1 > 0$, $\mathbf{y} > \mathbf{0}$ where

- 514 (i) The eigenvalue λ_1 is algebraically simple.
- 515 (ii) The eigenvalue λ_1 is dominant. That is, for any other eigenvalue μ of \mathbf{A} , $|\mu| < \lambda_1$.
- 516 (iii) The only nonnegative eigenvectors of \mathbf{A} are positive scalar multiples of \mathbf{y} .

517 By the Perron-Frobenius theorem we know that the spectral radius of a nonnegative primitive matrix is equal to the
 518 dominant eigenvalue of that matrix; $\rho(\mathbf{A}) = \lambda_1$. In our analysis we also make use of the Jordan canonical form for square
 519 matrices. We use this decomposition because while a nonnegative primitive matrix is not necessarily diagonalizable, every
 520 square matrix can none-the-less be written in its Jordan canonical form.

521 **Definition 7** For any square matrix \mathbf{A} , there exists a matrix \mathbf{J} such that

$$\mathbf{A} = \mathbf{P}\mathbf{J}\mathbf{P}^{-1}, \quad (133)$$

522 where \mathbf{J} is the Jordan canonical form of \mathbf{A} . The Jordan canonical form is a block diagonal matrix

$$\mathbf{J} = \begin{bmatrix} \mathbf{J}_1 & \dots & \mathbf{0} \\ \vdots & \ddots & \vdots \\ \mathbf{0} & \dots & \mathbf{J}_b \end{bmatrix}, \quad (134)$$

523 where each \mathbf{J}_i is called a Jordan block of \mathbf{A} . For Jordan block i , the diagonal entries are λ_i , the superdiagonal entries are
 524 one, and all other entries are zero.

525 Next, we present two lemmas that were used in the proofs of the main theorems. The first lemma was used in Theorem
 526 3.1 and bounds our initial condition for each neutral fraction i for each stage j , $v_{j,0}^i(x)$, sufficiently to establish the uniform
 527 convergence results for the neutral fractions.

528 **Lemma B.1** Let $x \rightarrow v_{j,0}^i(x)$ satisfy $x^2 v_{j,0}^i(x) e^{sx} \in L^1(\mathbb{R}) \cap L^\infty(\mathbb{R})$, then for each $s > 0$ there exists a positive constant
 529 C_j such that

$$w_{j,0}^i(x) = \frac{C_j e^{-sx}}{1 + x^2} \quad (135)$$

530 bounds $v_{j,0}^i(x)$ for all $x \in \mathbb{R}$. Moreover, the Fourier transform of $w_{j,0}^i(x) e^{sx}$ with respect to x is in $L^1(\mathbb{R})$ and is given by

$$C_j \pi e^{-|\omega|}. \quad (136)$$

531 For the proof of Lemma B.1, we refer the reader to Lemma 1 by Marculis et al. (2017).

532 We next provide a lemma that will be used in the proofs of the Theorems 3.2 and 3.3. In particular, we make use of
 533 the Jordan canonical form and the Perron-Frobenius theorem outlined above.

534 **Lemma B.2** Assume that the matrix \mathbf{B}_0 is nonnegative and primitive. Let λ_1 be the dominant eigenvalue of \mathbf{B}_0 , then

$$\lim_{t \rightarrow \infty} \left[\frac{\mathbf{B}_0}{\lambda_1} \right]^t = \mathbf{r}\boldsymbol{\ell} \quad (137)$$

535 where \mathbf{r} and $\boldsymbol{\ell}$ are the right and left eigenvectors corresponding to λ_1 respectively with $\boldsymbol{\ell}$ normalized by $\langle \boldsymbol{\ell}^T, \mathbf{r} \rangle$ to account
536 for the scaling in \mathbf{r} .

537 *Proof* Writing \mathbf{B}_0 in terms of its Jordan canonical form, we have

$$\lim_{t \rightarrow \infty} \left[\frac{\mathbf{B}_0}{\lambda_1} \right]^t = \lim_{t \rightarrow \infty} \left[\frac{\mathbf{P}\mathbf{J}\mathbf{P}^{-1}}{\lambda_1} \right]^t \quad (138)$$

$$= \lim_{t \rightarrow \infty} \frac{\mathbf{P}\mathbf{J}^t\mathbf{P}^{-1}}{\lambda_1^t}. \quad (139)$$

538 Since \mathbf{J} is block diagonal,

$$\mathbf{J}^t = \begin{bmatrix} \mathbf{J}_1^t & \dots & \mathbf{0} \\ \vdots & \ddots & \vdots \\ \mathbf{0} & \dots & \mathbf{J}_b^t \end{bmatrix}. \quad (140)$$

539 By the Perron-Frobenius theorem there exists a dominant eigenvalue λ_1 of \mathbf{B}_0 because \mathbf{B}_0 is nonnegative and primitive .
540 The first Jordan block is $\mathbf{J}_1 = [\lambda_1]$ and $\mathbf{J}_1^t = [\lambda_1^t]$. For Jordan block j of size $b_j \times b_j$ we have

$$\mathbf{J}_j^t = \begin{bmatrix} \lambda_j^t & \binom{t}{1}\lambda_j^{t-1} & \dots & \binom{t}{b_j-2}\lambda_j^{t-b_j+2} & \binom{t}{b_j-1}\lambda_j^{t-b_j+1} \\ 0 & \lambda_j^t & \dots & \binom{t}{b_j-3}\lambda_j^{t-b_j+3} & \binom{t}{b_j-2}\lambda_j^{t-b_j+2} \\ \vdots & \vdots & \ddots & \vdots & \vdots \\ 0 & 0 & \dots & \lambda_j^t & \binom{t}{1}\lambda_j^{t-1} \\ 0 & 0 & \dots & 0 & \lambda_j^t \end{bmatrix} \quad (141)$$

541 for $t \geq b_j - 1$. Since $|\lambda_j| < \lambda_1$, using L'Hôpital's rule, we have

$$\lim_{t \rightarrow \infty} \frac{\mathbf{J}_j^t}{\lambda_1^t} = \mathbf{0} \quad (142)$$

542 for $j = 2, \dots, b$. Returning to the Jordan canonical form,

$$\lim_{t \rightarrow \infty} \frac{\mathbf{J}^t}{\lambda_1^t} = \begin{bmatrix} 1 & \dots & 0 \\ \vdots & \ddots & \vdots \\ 0 & \dots & 0 \end{bmatrix}. \quad (143)$$

543 Hence from (139),

$$\lim_{t \rightarrow \infty} \frac{\mathbf{P}\mathbf{J}^t\mathbf{P}^{-1}}{\lambda_1^t} = \mathbf{P} \lim_{t \rightarrow \infty} \frac{\mathbf{J}^t}{\lambda_1^t} \mathbf{P}^{-1} \quad (144)$$

$$= \mathbf{P} \begin{bmatrix} 1 & \dots & 0 \\ \vdots & \ddots & \vdots \\ 0 & \dots & 0 \end{bmatrix} \mathbf{P}^{-1} \quad (145)$$

$$= \mathbf{r}\boldsymbol{\ell} \quad (146)$$

544 because \mathbf{r} is the first column vector of \mathbf{P} and $\boldsymbol{\ell}$ is the first row vector of \mathbf{P}^{-1} . Therefore, from (139) and (146),

$$\lim_{t \rightarrow \infty} \left[\frac{\mathbf{B}_0}{\lambda_1} \right]^t = \mathbf{r}\boldsymbol{\ell}. \quad (147)$$

The proof of Lemma B.2 is complete. \square

545 References

- 546 Austerlitz F and Garnier-Géré P. Modelling the impact of colonisation on genetic diversity and differentiation of forest
547 trees: interaction of life cycle, pollen flow and seed long-distance dispersal. *Heredity*, 90(4):282, 2003.
548 Bapat RB and Raghavan TE. Nonnegative matrices and applications, volume 64. Cambridge university press, 1997.
549 Bataillon TM, David JL, and Schoen DJ. Neutral genetic markers and conservation genetics: simulated germplasm col-
550 lections. *Genetics*, 144(1):409–417, 1996.

551 Bateman AW, Buttenschön A, Erickson KD, and Marculis NG. Barnacles vs bullies: modelling biocontrol of the invasive
552 european green crab using a castrating barnacle parasite. *Theor Ecol*, 10(3):305–318, 2017.

553 Bonnefon O, Garnier J, Hamel F, and Roques L. Inside dynamics of delayed travelling waves. *Math Mod Nat Phen*, 8:
554 44–61, 2013.

555 Bonnefon O, Coville J, Garnier J, and Roques L. Inside dynamics of solutions of integro-differential equations. *Discret*
556 *Contin Dyn Syst - Ser B*, 19(10):3057–3085, 2014.

557 Cooley JW and Tukey JW. An algorithm for the machine calculation of complex fourier series. *Math Comput*, 19(90):
558 297–301, 1965.

559 Cullingham CI, Cooke JE, Dang S, Davis CS, Cooke BJ, and Coltman DW. Mountain pine beetle host-range expansion
560 threatens the boreal forest. *Mol Ecol*, 20(10):2157–2171, 2011.

561 Davis MB and Shaw RG. Range shifts and adaptive responses to quaternary climate change. *Science*, 292(5517):673–679,
562 2001.

563 Easterling MR, Ellner SP, and Dixon PM. Size-specific sensitivity: applying a new structured population model. *Ecology*,
564 81(3):694–708, 2000.

565 Garnier J and Lewis MA. Expansion under climate change: the genetic consequences. *Bull Math Biol*, 78(11):2165–2185,
566 2016.

567 Garnier J, Giletti T, Hamel F, and Roques L. Inside dynamics of pulled and pushed fronts. *J des Math Pures Appl*, 98
568 (4):428–449, 2012.

569 Hallatschek O and Nelson DR. Gene surfing in expanding populations. *Theor Popul Biol*, 73(1):158–170, 2008.

570 Hastings A, Cuddington K, Davies KF, Dugaw CJ, Elmendorf S, Freestone A, Harrison S, Holland M, Lambrinos J,
571 Malvadkar U, et al. The spatial spread of invasions: new developments in theory and evidence. *Ecol Lett*, 8(1):91–101,
572 2005.

573 Hewitt G. The genetic legacy of the quaternary ice ages. *Nature*, 405(6789):907, 2000.

574 Holderegger R, Kamm U, and Gugerli F. Adaptive vs. neutral genetic diversity: implications for landscape genetics. *Landscape*
575 *Ecol*, 21(6):797–807, 2006.

576 Howe HF and Smallwood J. Ecology of seed dispersal. *Annu Rev Ecol Syst*, 13(1):201–228, 1982.

577 Ibrahim KM, Nichols RA, and Hewitt GM. Spatial patterns of genetic variation generated by different forms of dispersal
578 during range expansion. *Heredity*, 77(3):282, 1996.

579 Kot M, Lewis MA, and van den Driessche P. Dispersal data and the spread of invading organisms. *Ecology*, 77(7):
580 2027–2042, 1996.

581 Lefkovich L. The study of population growth in organisms grouped by stages. *Biometrics*, pages 1–18, 1965.

582 Leslie PH. On the use of matrices in certain population mathematics. *Biometrika*, 33(3):183–212, 1945.

583 Levin LA. Recent progress in understanding larval dispersal: new directions and digressions. *Integr Comp Biol*, 46(3):
584 282–297, 2006.

585 Lewis MA, Marculis NG, and Shen Z. Integrodifference equations in the presence of climate change: persistence criterion,
586 travelling waves and inside dynamics. *J Math Biol*, 77(6-7):1649–1687, 2018.

587 Li B, Lewis MA, and Weinberger HF. Existence of traveling waves for integral recursions with nonmonotone growth
588 functions. *J Math Biol*, 58(3):323–338, 2009.

589 Liebhold AM, Halverson JA, and Elmes GA. Gypsy moth invasion in north america: a quantitative analysis. *J Biogeogr*,
590 pages 513–520, 1992.

591 Lubina JA and Levin SA. The spread of a reinvading species: range expansion in the california sea otter. *Am Nat*, 131(4):
592 526–543, 1988.

593 Lui R. A nonlinear integral operator arising from a model in population genetics i. monotone initial data. *SIAM J Math*
594 *Anal*, 13(6):913–937, 1982a.

595 Lui R. A nonlinear integral operator arising from a model in population genetics ii. initial data with compact support.
596 *SIAM J Math Anal*, 13(6):938–953, 1982b.

597 Lui R. Existence and stability of travelling wave solutions of a nonlinear integral operator. *J Math Biol*, 16(3):199–220,
598 1983.

599 Lui R. Biological growth and spread modeled by systems of recursions. i. mathematical theory. *Math Biosci*, 93(2):269–295,
600 1989a.

601 Lui R. Biological growth and spread modeled by systems of recursions. ii. biological theory. *Math Biosci*, 93(2):297–311,
602 1989b.

603 Lutscher F and Lewis MA. Spatially-explicit matrix models. *J Math Biol*, 48(3):293–324, 2004.

604 Marculis NG and Lui R. Modelling the biological invasion of *carcinus maenas* (the european green crab). *J Biol Dyn*, 10
605 (1):140–163, 2016.

606 Marculis NG, Lui R, and Lewis MA. Neutral genetic patterns for expanding populations with nonoverlapping generations.
607 *Bull Math Biol*, 79(4):828–852, 2017.

608 Moloney KA. A generalized algorithm for determining category size. *Oecologia*, 69(2):176–180, 1986.

609 Neubert MG and Caswell H. Demography and dispersal: calculation and sensitivity analysis of invasion speed for structured
610 populations. *Ecology*, 81(6):1613–1628, 2000.

611 Pluess AR. Pursuing glacier retreat: genetic structure of a rapidly expanding *larix decidua* population. *Mol Ecol*, 20(3):
612 473–485, 2011.

613 Roques L, Hosono Y, Bonnefon O, and Boivin T. The effect of competition on the neutral intraspecific diversity of invasive
614 species. *J Math Biol*, 71(2):465–489, 2015.

615 Roques L, Garnier J, Hamel F, and Klein EK. Allee effect promotes diversity in traveling waves of colonization. *Proc Natl*
616 *Acad Sci*, 109(23):8828–8833, 2012.

617 Vandermeer J. Choosing category size in a stage projection matrix. *Oecologia*, 32(1):79–84, 1978.

618 Veit RR and Lewis MA. Dispersal, population growth, and the allee effect: dynamics of the house finch invasion of eastern
619 north america. *Am Nat*, 148(2):255–274, 1996.

620 Weinberger HF. Asymptotic behavior of a model in population genetics. In *Nonlinear Partial Differential Equations and*
621 *Applications*, pages 47–96. Springer, 1978.

622 Weinberger HF. Long-time behavior of a class of biological models. *SIAM J Math Anal*, 13(3):353–396, 1982.